This is a preprint, the final version is subject to change, of the American Mineralogist (MSA)
Cite as Authors (Year) Title. American Mineralogist, in press.
(DOI will not work until issue is live.) DOI: http://dx.doi.org/10.2138/am-2017-5928

REVISION 1

Magma mush chemistry at subduction zones, revealed by new melt major element inversion from calcic amphiboles

JING ZHANG[1,2], MADELEINE C.S. HUMPHREYS[1,*], GEORGE F. COOPER[1], JON P. DAVIDSON[1], AND COLIN G. MACPHERSON[1]

[1]Department of Earth Sciences, Durham University, Durham, DH1 3LE, UK

[2]State Key Laboratory of Lithospheric Evolution, Institute of Geology and Geophysics, Chinese Academy of Sciences, Beijing, 100029, China

* E-mail: madeleine.humphreys@durham.ac.uk

In memory of our friend and colleague, Jon Davidson

ABSTRACT

We have used multiple-regression methods to calibrate new, pressure-independent empirical chemometric equations to calculate the major element composition of basanitic to rhyolitic melts in equilibrium with calcic amphibole. The equations are based on amphibole stoichiometric formula components ± temperature from published experimental P-T-X data, and avoid some problems of previous studies associated with uncertainties in pressure determination. Compared with the pressure-dependent equations of Ridolfi and Renzulli

(2012), tests run using an independent dataset indicate that the new equations yield improved precision and accuracy, in particular for SiO_2, TiO_2, CaO and K_2O. The results are only marginally more precise when temperature is used as a dependent variable, demonstrating that temperature has a relatively minor role in controlling amphibole crystal chemistry compared with melt composition. This allows us to accept a small decrease in precision in excluding temperature from the analysis, which is very convenient for application of the equations to natural amphiboles where temperature is typically unknown.

Using the new chemometric equations, reconstructed melt compositions in equilibrium with the rims of amphiboles in pumice clasts of the Ongatiti ignimbrite are in good agreement with coexisting matrix glass compositions, lending support for our analysis. The compositionally variable cores of the amphiboles give predicted melt compositions with large compositional variations from andesitic (63 wt% SiO_2) to high-Si rhyolite. These compositional variations in the predicted melt compositions suggest that there may be a range of heterogeneous melts undergoing progressive differentiation within a major crustal magma storage region underneath the volcano. The results support the existence of genuine intermediate composition melts within the storage region. Interaction between these stored melts, disaggregating mush fragments and replenishing magmas gives rise to the chemical complexity observed in erupted magmas. We also used our multiple regression model to predict melts that were in equilibrium with amphiboles in plutonic nodules from Grenada lavas. The predicted melts cover a wide range of compositions, perhaps as a result of in situ fractionation, but are consistent with melt inclusions hosted in those cumulates, as reported by Stamper et al. (2014). Overall, our new pressure- and temperature-independent equations resolve issues associated with previous pressure-dependent studies and represent a useful tool for further investigation of crustal processes at subduction zones.

Keywords: Calcic amphibole, chemometrics, melt compositions, multiple regression, Ongatiti ignimbrite, plutonic xenoliths, Grenada.

INTRODUCTION

Amphibole is a common, but chemically complex mineral phase present in many hydrous arc magmas. Experimental studies show that amphibole crystallises over a large range of pressure and temperature from diverse melts of basanitic to rhyolitic composition (see below; Fig. 1a-d). The crystal chemistry of amphibole is sensitive to various magma intensive variables (e.g. pressure, temperature, oxygen fugacity fO_2), as well as melt composition and volatile content (e.g. Ridolfi and Renzulli 2012; Ridolfi et al. 2008, 2010). Because of its broad stability range, amphibole has long been used for thermobarometry (e.g. Anderson and Smith 1995; Blundy and Cashman 2008; Blundy and Holland 1990; Ernst and Liu 1998; Hammarstrom and Zen 1986; Holland and Blundy 1994; Hollister et al. 1987; Krawczynski et al. 2012; Molina et al. 2015; Putirka 2008, 2016; Ridolfi and Renzulli 2012; Ridolfi et al. 2010; Schmidt, 1992). To begin with, amphibole-related barometers were mainly based on the presence of a low-variance equilibrium assemblage. For example, the Al-in-hornblende barometer requires the assemblage quartz + K-feldspar + plagioclase + hornblende + biotite + Fe-Ti oxides + titanite + melt + fluid (e.g. Anderson and Smith 1995; Hammarstrom and Zen 1986; Hollister et al. 1987). More recently, empirical amphibole-only thermobarometers have been produced (Ridolfi and Renzulli 2012; Ridolfi et al. 2010), but application of these barometers is limited by large offsets (e.g. up to 1,100 MPa) between predicted pressure and experimental pressure (e.g. Erdmann et al. 2014; Putirka 2016; Shane and Smith, 2013). This suggests that amphibole crystal chemistry is more sensitive to temperature and melt composition than to pressure (Putirka 2016).

The same empirical thermobarometric formulations have been used to describe the links between amphibole crystal chemistry and anhydrous melt major element composition, using chemometric equations (Ridolfi and Renzulli 2012; see Eqs 5-11 therein). These (pressure-dependent) empirical relationships enable melt SiO_2, TiO_2, Al_2O_3, FeO, MgO, CaO and K_2O contents to be calculated from knowledge of amphibole major element formula proportions and pressure. However, for natural igneous amphiboles, pressure is rarely known independently, and given the uncertainty in pressures estimated from amphibole-only barometer models (e.g. Ridolfi and Renzulli 2012) this could cause large uncertainties in the inferred melt compositions. Furthermore, although Erdmann et al. (2014) demonstrate that Ridolfi and Renzulli (2012)'s model yields reasonable melt SiO_2 content estimates for calcic amphiboles crystallized from experimental melts with 55-75 wt % SiO_2 content, for calcic amphiboles crystallized from more mafic melts, melt SiO_2 is overestimated by up to 15 wt % (see below). Similar issues also exist in calculating melt TiO_2, FeO, CaO and K_2O contents. Finally, although magma temperature is somewhat easier to determine petrologically than pressure, temperature is also typically an unknown so we would ideally want to reconstruct melt composition in the absence of both temperature and pressure terms.

In this study we have compiled an expanded dataset of previously published experimental studies that crystallised amphibole. Using multiple regression analysis, we then re-examine the compositional relationships between amphibole and melt, and generate new chemometric equations with improved accuracy for SiO_2, TiO_2, FeO, CaO and K_2O, compared with Ridolfi and Renzulli (2012). The accuracy of our chemometric equations is tested using a second, independent experimental dataset. Importantly, our formulations are independent of pressure and we propose models both with and without temperature terms. This brings significant advantages in application of the equations to natural systems. We apply the new equations to infer melt compositions coexisting with amphiboles erupted in the

Ongatiti ignimbrite, Taupo Volcanic Zone, New Zealand, and with plutonic amphiboles preserved in xenoliths erupted from Grenada, Lesser Antilles.

SELECTING P-T-X DATA FROM LITERATURE

Experimental data from the Library of Experimental Phase Relations (LEPR) database (Hirschmann et al. 2008) and other studies were considered. We first split the data into two groups (Fig. 1a, c): one group for calibration (n=130, Table 1); and one group for test (n= 74, Table 1). The split of the experimental data from different references is random, and the two groups cover the same range of experimental P-T run conditions, melt compositions and the crystal chemistry of the experimentally produced amphiboles (except that the test group lacks kaersutite), demonstrating good representativeness of the test group. The calibration group also overlaps those datasets used in the previous studies of Ridolfi and Renzulli (2012) and Erdmann et al. (2014) (Table 1), whereas none of the data from the test group were used in these studies. Therefore, the test group can also be used as a direct, independent test of Ridolfi and Renzulli (2012)'s results. We applied two criteria to filter the data (see below): 1) the amphibole compositions must be calcic according to International Mineralogical Association (IMA; Hawthorne et al., 2012); 2) there must be amphibole-melt equilibrium as tested using the Fe-Mg exchange coefficient.

First, all the selected amphibole compositional data from the literature were recalculated from wt% oxide to formula proportions (atoms per formula unit/apfu), following the amphibole stoichiometry calculation procedure recommended by IMA (Leake et al. 1997). Si, Al, Ti, Cr, Fe, Mn, Mg were allocated to the tetrahedral (T) and small octahedral (M1-3) sites and Fe^{3+} and Fe^{2+} proportions were determined separately by charge balance, taking the approach of "average Fe^{3+}" as described by Schumacher (1997). This is important because the details of the ferric-ferrous calculations can affect other formula components, including

119 Na_{M4} and thus A-site totals. Ca, Na and K were allocated to the large octahedral (M4) and
120 vacant/partially-filled (A) sites. Any amphiboles classified as non-calcic (Ca_{M4} < 1.5 apfu)
121 were discarded. The remaining calcic amphiboles are classified as edenite-pargasite (Parg),
122 hastingsite-magnesiohastingsite (MgHst), kaersutite - ferrokaersutite (Kaer), tschermakite-
123 ferrotschermakite (Tsch) and magnesiohornblende (MgHbl) following Leake et al. (1997)
124 (Table 1; Fig. 2). Amphiboles that failed to meet the standard of stoichiometry calculation of
125 calcic amphibole were also discarded at this point.

126 Second, following Putirka (2016), we employed the Fe-Mg exchange coefficient
127 $K_D(\text{Fe-Mg})^{\text{Amph-melt}}$ (simply K_D) to test whether equilibrium was achieved between
128 amphiboles and coexisting melts during the experiments. K_D, expressed as:

$$K_D = \frac{X_{FeOt}^{Amph}}{X_{MgO}^{Amph}} \Big/ \frac{X_{FeOt}^{Melt}}{X_{MgO}^{Melt}}$$

129 (FeOt is total Fe as FeO). K_D is independent of temperature, pressure and co-crystallizing
130 mineral phases (Putirka, 2016). Following Putirka (2016), we consider K_D values in the range
131 of 0.28±0.11 as an indication of equilibrium. Any experimentally produced amphibole and
132 melt compositions that fell outside this range were removed from the dataset (Fig. 3); we note
133 that the samples that failed to meet this test for equilibrium did not fall into any particular
134 range of experimental P-T conditions or melt chemistry (Fig. 1).

135 **CALCIC AMPHIBOLE CRYSTALLIZATION CONDITIONS**

136 The resultant dataset of experimental calcic amphiboles shows wide compositional
137 variability ($5.7 < Si_T < 7.0$; $0 < Ti_{M1\text{-}3} < 0.8$; $0 < [Na+K]_A < 1.0$) over the range of
138 experimental conditions (Fig. 2). The experimental dataset generally represents amphibole
139 crystallization conditions in an evolving magmatic environment, from hot, mafic melt (950-

1,100 °C, c.a. 40-60 wt % SiO_2) to cooler, felsic melt (800-950 °C, c.a. 60-78 wt % SiO_2) (Fig. 1c-d). Exceptions to this trend are present as outliers, for example the crystallisation of MgHbl from rhyolitic melts at temperatures up to 1050 °C (Sisson 1994) (Fig. 1d). We did not examine the effect of variations in melt H_2O concentration or oxygen fugacity in this study. At low pressure, the crystallization of calcic amphiboles occurs over a large temperature range (750-1,050 °C) while at high pressure conditions (2-2.5 GPa) this range narrows and calcic amphiboles are linked to the highest temperatures (1,050-1,100 °C; Fig. 1b). This limitation is not unique to our dataset and was recognised by Ridolfi and Renzulli (2012). To some extent this range of conditions may reflect the stability of calcic amphiboles and the liquid line of descent of evolving magmas (Ridolfi and Renzulli 2012; Ridolfi et al. 2010), but may also simply represent the conditions of interest for recent experimental studies.

The crystallisation conditions of individual amphibole species are shown in Fig. 1d (pressure and temperature) and Fig. 4 (melt chemistry). Parg and MgHst dominate in the hottest, most mafic melts, while MgHbl is found only in cooler, more silicic melts (typically > 70 wt% SiO_2). Kaer crystallizes from melts with similar SiO_2 and Al_2O_3 contents to those MgHst-bearing melts, but with higher TiO_2 and lower CaO and MgO contents (Fig. 4a-b, d-e). The compiled dataset also demonstrates that MgHst, MgHbl and Tsch can all crystallize at the same pressure (e.g. 200 MPa; Fig. 1b). The poor correlation between pressure and amphibole tetrahedral Si and Al content (Si_T and Al_T, respectively) demonstrates the weak control by pressure on amphibole crystal chemistry (Putirka 2016); in contrast, amphibole Si_T is strongly correlated with melt SiO_2 and TiO_2 contents (e.g., Fig. 1f), and intermediately correlated with temperature (Fig. 1e), suggesting that melt compositions and temperature are more important controlling factors to amphibole compositions than pressure. The stronger correlation of amphibole Si_T against melt SiO_2 content than against temperature also indicates

that melt chemistry is probably more important than temperature in controlling amphibole crystal chemistry (Putirka 2016).

MULTIPLE REGRESSION ANALYSIS

In order to investigate the relationships between melt major element compositions and amphibole crystal chemistry and temperature, we carried out a multiple regression (MR) analysis using the statistical software package R (R Core team 2013). The MR analysis allows the values of dependent variables to be predicted based on multiple input parameters (independent variables). The SiO_2, TiO_2, Al_2O_3, FeO, MgO, CaO, K_2O contents in the melt, normalized to 100% anhydrous, are treated as dependent variables. We initially inspected the entire calibration dataset and noticed that melt TiO_2, FeO, MgO, CaO all showed curving relationships with amphibole formula components; therefore we decided to use the natural logarithms of the concentration (e.g. $lnTiO_2$, melt) as dependent variables. Failure to do this may yield negative calibration results at low concentrations. Similarly, for melt SiO_2 we identified a curving relationship with Si_T (amph) and therefore used $ln(Si_T)$ as an independent variable for regression against melt SiO_2. For independent variables, we tested both amphibole-only and amphibole+T approaches, in order to decipher the significance of temperature in controlling amphibole crystal chemistry. The MR analyses were performed independently of pressure. Rather than using total formula proportions unassigned to different crystallographic sites (Ridolfi and Renzulli 2012), as independent compositional variables we used the stoichiometric components, including tetrahedral site Si (Si_T), M1-3 site Al (Al_{VI}), Fe^{3+}, Mg, Ti and Fe^{2+}, and M4 site Ca (Ca_{M4}), and A site Na (Na_A). We also tested regressions using Fe_T instead of ferric and ferrous components because of the uncertainties associated with calculation of Fe^{3+} and Fe^{2+} (Schumacher 1997), although with only one exception this did not appear as a significant parameter. Tetrahedral site Al (Al_T), which has

188 commonly been treated as one of the key parameters in previous amphibole thermobarometry
189 studies, was avoided as an independent variable, in order to avoid the issue of
190 multicollinearity. This is because amphibole SiO_2 or Si_T are strongly correlated with melt
191 SiO_2 content (e.g. Fig. 1f), and the stoichiometric calculation method uses Al_T to fill the
192 tetrahedral site after accommodation of all available Si ($Si_T + Al_T = 8$ apfu), with excess Al
193 assigned to the octahedral sites (M1-3). We also did not consider Na_{M4}, for a similar reason
194 (Ca + Na = 2 apfu in M4, with excess Na assigned to the A site). We did not consider M1-3
195 site Cr and Mn, and A-site K, due to their minor abundances in amphibole and thus high
196 relative analytical uncertainties.

197 The output of each MR analysis is given as the intercept and coefficients of the
198 nominated independent variables, on which basis a multiple regression function can be
199 derived (Table 2). For example, *Eq. 1* used for calculating the SiO_2 content in the melt is
200 written as:

$$SiO_2\ (wt\ \%) = -228.000 - 0.0107T + 165.000\ \ln Si - 7.2190Mg \quad (Eq.\ 1)$$

201 Evaluation of each function was done based on the coefficient of determination (R^2),
202 standard error of the estimate (*SE*), number of objects/observations (*N*), and confidence of the
203 coefficients for each independent variable and constant (*p-value*). A correlation that we deem
204 to be statistically significant is reflected by $N \geq 30$, $R^2 \geq 0.6$ and *p-value* of each determined
205 coefficient < 0.01. In preference, we chose equations with fewer variables as this reduces the
206 propagated analytical uncertainty in applying the regressions to natural data. In Table 2, we
207 use the normal font to denote that the *p-values* of the MR-derived independent variables and
208 the constants are < 0.01 (>99% confidence), the bold font to denote that the *p-values* of the
209 corresponding independent variable/constant are in the range 0.01-0.03 (97-99% confidence).
210 The MR analysis was performed following a trial-and-error procedure: all independent

variables mentioned above were initially included in the MR analyses, then those with highest *p-value* > 0.01 were progressively removed until all the remaining independent variables and constants are statistically significant (mostly *p-value* <<0.01 in our calibrations).

We use the standard error of estimate (*SE*) to denote the precision of chemometric equations derived from MR analyses (Table 2). This is done by comparison of the predicted and measured data from the calibration dataset. To test the accuracy of the results, we applied the MR-derived equations to amphiboles from the test dataset to predict the compositions of their coexisting melts. Equivalent statistical parameters calculated for comparison of the test group with experimental melt compositions are denoted using lower case (e.g. r^2, *se*; Table 2) and are compared with those of the MR analysis. We regard *se* values (in wt % oxide) of corresponding chemometric equations as representative of the accuracy of the MR analyses, although *se* is typically lower than SE because of the more restricted compositional spread of the test dataset.

RESULTS

The major element compositions of the experimental melts can, in general, be linked with amphibole formula components ± experimental run temperature with robust R^2 (typically > 0.70) and reasonable precision (*SE*) and accuracy (*se*) (Table 2). In many cases, no statistically robust T-dependent parameterisation could be found. Otherwise, as expected, the addition of temperature as an independent variable slightly improves the precision of the MR equations, as revealed by decreasing *SE* and *se*, compared to those without including temperature as an independent variable (e.g. decrease of *SE* from 0.68 to 0.60 in the prediction of $\ln TiO_2$, *Eq. 5-6,* Table 2).

Moreover, our MR analyses results demonstrate the variable significance of amphibole major element formula proportions as the independent variables. Agreement of melt compositions of our calibration and test groups with experimental melt compositions is improved compared to Ridolfi and Renzulli (2012)'s study, which uses the total formula proportions of the major elements unassigned to different crystallographic sites, e.g. Al_{total} instead of Al_T and Al_{VI}, Fe_{total} instead of Fe^{2+} and Fe^{3+}, Na_{total} instead of Na_{M4} and Na_A (see greater details below).

Melt SiO_2 content can be predicted robustly with two main groups of independent variables: lnSi + Al_{VI} + Fe^{3+} + Fe^{2+} + Ti + Ca ± Na_A ± Mg (*Eq. 1-2*), and lnSi + Mg ± T (*Eq. 3-4*). The melt SiO_2 contents of the test data are reproduced very well with $R^2 \geq 0.78$ (Fig. 6a), but in particular, the new equations are able to reproduce experimental melts with low SiO_2 contents (<55 wt%, data from Adam and Green 2006, Adam and Green 1994, Adam et al. 1993, Dalpé and Baker 2000, and Fujinawa and Green 1997), which failed to be reproduced with Ridolfi and Renzulli (2012)'s equations (Fig. 6a). One temperature-dependent equation was produced for Si and this brings only marginal increased precision and accuracy (*Eq.* 3, Table 2).

The natural logarithm of melt TiO_2 content can also be predicted robustly with the following group of independent variables: Si + Al_{VI} + Fe^{3+} + Fe^{2+} + Ca + Na_A ± T (Mg-absent group; *Eq. 5-6*). In general, the calibration results and test results are in excellent agreement with experimental melt TiO_2 content ($R^2 > 0.8$, Fig. 6b). The standard error is significantly smaller for the test population of data points and this is probably because of the more limited compositional range of amphiboles in this dataset (see Table 1). As for SiO_2, our equations also manage to reproduce the TiO_2 content of both calibration and test data points from the

256 experiments with low melt SiO_2 content, where Ridolfi and Renzulli (2012)'s equation
257 generates a large offset (cluster of points at ~ 2 wt% TiO_2, Fig. 6b).

258 The natural logarithm of melt FeO content can be predicted with two different groups
259 of independent variables: Si + Al_{VI} + Fe^{3+} + Fe^{2+} + Ti + Ca (Mg-absent group; *Eq. 7*) and Si +
260 Mg + Ca (*Eq. 8*). The calibrations are less robust than those for SiO_2 and TiO_2 (R^2 ~ 0.70)
261 and no robust temperature-dependent regression was identified. The overall accuracy of our
262 FeO calibrations is similar to that of Ridolfi and Renzulli (2012), but with similar
263 improvements in accuracy for melts with high FeO content (Fig. 6c), as for SiO_2 and TiO_2
264 (above).

265 Pressure is a very significant independent variable in Ridolfi and Renzulli (2012)'s
266 model for melt MgO content (Fig. 5). At pressures >1 GPa (as calculated by Ridolfi and
267 Renzulli (2012)'s barometer model), the predicted melt MgO is exponentially controlled by
268 pressure, leading to drastic overestimation of melt MgO (Fig. 5). Even when the calculated
269 pressure is <1 GPa and in good agreement with the experimental pressure, their calibration
270 still generates significant scatter to high predicted melt MgO content (Fig. 5, 6g-h). In
271 contrast, the results of our MR analyses suggest that the natural logarithm of melt MgO
272 content can be predicted robustly with the independent variables Si + Al_{VI} + Mg (*Eq.9*; Fig.
273 6d), although, as for FeO, no robust T-dependent regression was identified. This small
274 number of independent variables is in contrast with the model of Ridolfi and Renzulli (2012),
275 which uses all amphibole major elements and pressure as independent variables. Our P-
276 absent MgO predictions are very similar to those of Ridolfi for melts with MgO < 2 wt% but
277 appear to be in much greater agreement with both calibration and test data for melts with
278 higher MgO contents (R^2 = 0.80) than those of RR2012 (Fig. 6d).

For pressures > 1 GPa, as calculated using Ridolfi and Renzulli (2012)'s barometer, their equation for predicting melt CaO content produces a significant proportion of negative melt CaO contents. Our calibrations significantly improve the accuracy of predicted melt CaO content, particularly for more primitive melts and those at higher pressures (e.g. R^2 = 0.71, *Eq. 11*; Fig. 6e). We derive two groups of calibrations using CaO content and lnCaO, respectively; both groups are related to Si + Mg ± Al_{VI} ± Na_A (*Eq,* 10, 11). The two groups of calibrations generate results that are in good agreement with each other except at high melt CaO contents, where *Eq. 10* starts to significantly underestimate CaO relative to the measured values; on balance, despite some scatter *Eq, 11* performs better over a wider range of compositions (as reflected by lower SE and higher R^2, Table 2; Fig. 6e).

Ridolfi and Renzulli (2012)'s equation for predicting melt K_2O content fails to reproduce the test and calibration data points from the low-melt SiO_2 content experiments, as for other elements (above), leading to significant over-estimation of melt K_2O for these compositions (Fig. 6f). In comparison, our calibrations give significant improvements in precision and accuracy for K_2O content in the experimental melts (R^2 = 0.628; *SE* = 0.59 wt %; *se* = 0.78 wt%; *Eq. 12, Fig. 6f*, Table 2), using Si + Al_{VI} + Mg + Fe^{3+} + Fe^{2+} + Ti + Ca + Na_A We also retrieved a robust regression using the parameter set Si+ Fe_T + Ti + Ca (*Eqn 13* although this has significantly lower predictive power (R^2 = 0.43, table 2). However, our *Eq. 12* still tends to underestimate melt K_2O at higher melt K_2O contents (> 3.0 wt %), with a small subset of otherwise apparently typical data plotting at anomalously low predicted melt K_2O (Fig. 6f).

For prediction of melt Al_2O_3 content, our best calibration is achieved using Al_{VI} + Mg + Fe^{3+} + Ti + Na_A (*Eq. 14*; Table 2). However, our calibration performs similarly to that of Ridolfi and Renzulli (2012) (R^2 = 0.59, SE = 0.93 wt%, Fig. 6g).

We did not find any robust regressions with an acceptable R^2 for melt Na_2O content; this finding is consistent with Ridolfi and Renzulli (2012) and we therefore do not attempt to predict melt Na_2O. We speculate that this lack of robust correlation could be due to problems with accurate electron microprobe analysis of Na in glass (Ridolfi and Renzulli 2012), or may arise if variable crystallisation of plagioclase from the host melts controls melt Na_2O content.

The *se* values for the test data are generally larger than *SE* for the calibration dataset, except for estimation of $lnTiO_2$, lnFeO and lnMgO. This is partly due to the smaller number of analyses in the test group (n = 74 compared with n = 130 for the calibration group) and likely also in part because the range of melt TiO_2, FeO and MgO of the test experiments is slightly smaller than the calibration experiment group (with a slightly different balance of amphibole species, Table 1). The calibrations of melt K_2O and Al_2O_3 contents are the least robust among all calibrated elements (R^2 = 0.59 and 0.63, respectively, with high relative *SE* and *se Eq. 12-14*). In general, the effect of excluding temperature as an independent variable appears to be minimal, with no loss in accuracy over temperature-dependent results. This is important because the absence of both temperature and pressure in our calibrations is a major advantage in applying our results to natural systems, in which they are typically unknown.

IMPLICATIONS

Here we present two case studies to demonstrate how our chemometric equations may be applied to both volcanic and plutonic amphiboles: amphiboles in pumice clasts from the Ongatiti ignimbrite of Mangakino volcano, and in plutonic nodules from Grenada lavas.

Applications to amphiboles from the Ongatiti ignimbrite

Background The Ongatiti ignimbrite was erupted from Mangakino volcano, Taupo volcanic zone, New Zealand, at around 1.2 Ma (Houghton et al. 1995). The following

summary is taken from the recent study of Cooper and Wilson (2014). The ignimbrite represents a large (>500 km^3 dense rock equivalent) unzoned deposit of crystal-rich rhyodacite to rhyolite magma, containing 20-30% crystals of plagioclase, quartz, orthopyroxene, amphibole, Fe-Ti oxides, zircon and apatite. Amphibole crystals from pumice clasts of the Ongatiti ignimbrite show variations in mineral textures coupled with varying chemical compositions. The majority of the amphiboles (83%) have resorbed, patchy zoned cores (Type B crystals), in contrast to Type A crystals, which are unzoned or only weakly zoned. Both Types have oscillatory zoned, relatively homogeneous rims with similar composition to the Type A cores (MgHbl, $1.20 < Al_T < 1.42$; Fig. 7b, c). Type B cores have heterogeneous major and trace element compositions ($1.16 < Al_T < 2.10$, dominantly MgHst and MgHbl compositions with rare Tsch-Parg). The amphiboles coexist with homogeneous rhyolitic matrix glass (SiO_2 = 77.75 -78.63 wt %; Table 3; Fig. 8). It is suggested that the resorbed Type B amphibole cores were sourced from chemically variable crystal mushes that were disaggregated and transported by a later melt replenishment event, and brought into a final shallow storage region, where additional amphibole crystallisation occurred to form the Type A amphiboles and oscillatory zoned overgrowths (Cooper and Wilson 2014). In the following analysis we first assess the degree to which our amphibole chemometric equations can reproduce the major element compositions of matrix glasses. We then apply our equations to infer the chemical compositions of the mush melts from which the Type B cores grew, prior to disaggregation and possible partial dissolution during transport to the melt-dominant body.

Testing for reproduction of equilibrium matrix glass compositions The crystal rims of all amphiboles from Ongatiti are chemically homogeneous and textural evidence indicates that they are also in equilibrium with the matrix glass (Cooper and Wilson 2014). We therefore focus on attempting to reconstruct the compositions of matrix glasses in

equilibrium with the rims of amphiboles from selected pumice clasts (GC1, P2023, P2026, P2027 and P2184, see Table 3; Cooper and Wilson 2014) using the temperature-independent equations from Table 2. The resulting predicted melt compositions are given in Table 3 and plotted in Fig. 8. In general, the calculated melt compositions agree well with the measured matrix glass compositions, within the *SE* of the corresponding MR equations. Predicted Al_2O_3 compositions are in less good agreement, systematically ~1.5 wt% higher than those of the measured matrix glass compositions. This is probably related to the overestimation of melt Al_2O_3 with *Eq. 19* at low melt Al_2O_3 content (see Fig. 6g). We note that the predicted melt CaO, MgO and FeO concentrations are in very good agreement with the low-SiO_2 end of the spread of measured glass compositions. This could be explained if the amphibole equilibrated with the melt before minor microlite crystallisation took place. Overall, the results demonstrate good reliability of our chemometric equations in predicting melt major element compositions and supports the conclusion derived by Cooper and Wilson (2014)'s study that the homogeneous rims of amphiboles are in equilibrium with the melts prior to the eruption.

Predicted melt compositions in equilibrium with amphibole cores We now use our MR-derived chemometric equations to predict the compositions of melts in equilibrium with the cores of Type B amphiboles, which display complex patchy zoning texture and large compositional variations and were inferred to have formed in a chemically heterogeneous crystal mush (Cooper and Wilson 2014). The results are plotted in Fig. 8 and indicate that the cores of Ongatiti Type B amphiboles are nominally in equilibrium with melts spanning a large compositional range from ~63-80 wt % SiO_2, 0.1-0.7 wt% TiO_2, ~1-5 wt% FeO and ~2-5 wt % K_2O (Fig. 8). The inferred melts form an array comprising two groups as a result of the presence of both MgHbl (with >44 wt% SiO_2 and < 9 wt% Al_2O_3) and MgHst (with <44 wt% SiO_2 and typically > 10 wt% Al_2O_3) within the Type B cores. Our key assumption is

that each amphibole analysis remained in equilibrium with the melt from which it crystallised and therefore represents a snapshot of past melts that may no longer exist. However, some of the crystal cores show gradational variations in greyscale in BSE images (see Fig. 7b) that could represent partial solid-state diffusive equilibration. Before making any petrogenetic interpretations about the inferred snapshot melt compositions we must therefore exclude the possibility that any significant Fe-Mg interdiffusion may be modifying the predicted melt compositions.

Intra-grain Fe-Mg diffusion could affect the validity of calculated melt compositions because both Mg_{M1-3} and Fe_{M1-3} may be present in the chemometric equations, and have different coefficients (see Table 2). At this stage, we exclude significant diffusion in other elements because, although very few diffusivity data for amphibole are currently available, comparison with olivine, clinopyroxene and orthopyroxene suggests that Fe-Mg interdiffusion is orders of magnitude quicker than for other elements (Allan et al. 2013). In order to quantify the potential variation in calculated melt compositions that might arise in response to Fe-Mg interdiffusion, we take two amphibole core compositions as examples (Fig. 8). The initial compositions are a MgHst with 41.83 wt% SiO_2, 11.62 wt% Al_2O_3 and molar Mg# 0.67, and a MgHbl with 44.65 wt% SiO_2, 7.66 wt% Al_2O_3 and Mg# 0.57 (see Table 4). We then arbitrarily modify their Mg# within the observed range in the natural amphibole dataset (0.90 to 0.10) and recalculate the predicted melts. The results are shown as vectors in Fig. 8. The diffusion-related variations fall close to the arrays of predicted melts for TiO_2, CaO, K_2O and MgO (Fig. 8a, d, e, f), but cut across the arrays for melt FeO and Al_2O_3 (Fig. 8b, c). This suggests that Fe-Mg interdiffusion is not extensive amongst the Ongatiti amphiboles, otherwise the calculated melt compositions would show scattered variations in Fe and Al. Although some effect of minor Fe-Mg interdiffusion is possible within the uncertainties of the predicted melt compositions, it is clear that the full range of predicted

401 melts far exceeds any apparent variability that could arise due to diffusion. We therefore take
402 confidence in the calculated melt compositions inferred to have been in equilibrium with the
403 amphibole cores.

404 Cooper and Wilson (2014) concluded that the large compositional diversity in
405 Ongatiti amphiboles is related to compositional variations in heterogeneous crystal mushes
406 over a range of pressure-temperature conditions. Our analysis supports this hypothesis, and
407 suggests that the MgHst amphibole cores crystallised from less evolved melts with 63-70 wt%
408 SiO_2 and 2.5-5 wt% FeO. The patchy texture (Figure 5 of Cooper and Wilson 2014) probably
409 arises by partial dissolution during ascent with the replenishing magma (e.g. Humphreys et al.
410 2006a) and new MgHbl then starts to crystallise from the eventual melt which has an initial
411 composition of ~73 wt% SiO_2 and 2 wt% FeO. Further differentiation of the replenishing
412 magma during shallow storage gives rise to increasingly silicic melts with >73 wt% SiO_2 (Fig.
413 8).

414 Our analysis therefore suggests that the Mangakino crustal storage region hosted
415 progressively differentiated melts of andesitic (~63 wt% SiO_2) to rhyolitic composition.
416 Within uncertainty, there is an almost continuous spread of inferred compositions and no
417 significant compositional gap; however the compositions of the predicted melts are bimodal
418 in abundance (Fig. 8). Our inferred melts are consistent with the compositions of a global
419 dataset of arc melt inclusions, but represent melts that are rarely sampled in the melt inclusion
420 record (60-70 wt% SiO_2, Reubi & Blundy 2009). This interpretation is interesting because it
421 is in contrast with a wealth of previous studies that suggested that andesites are largely a
422 result of mixing between mafic and silicic magmas, combined with mechanical incorporation
423 of a crystal load (e.g. Eichelberger et al. 2006; Humphreys et al. 2006a; Reubi and Blundy
424 2009). However, the andesitic melts in the Mangakino volcanic plumbing system are
425 probably short-lived and are not sampled by eruption at the surface. Without further textural

information linked explicitly to measured amphibole compositions we cannot comment further on the likely spatial or temporal distribution of the varying melt compositions within the heterogeneous crystal mush beneath Mangakino volcano. However, this approach seems worthy of further investigation as an alternative means to examine the nature of crustal storage and melt differentiation in arcs.

Applications to amphiboles in plutonic xenoliths from Grenada

Our second case study for application of the new chemometric equations is that of the abundant plutonic xenoliths erupted in lavas from Grenada, Lesser Antilles, as described by Stamper et al. (2014) and summarised below. The xenoliths are dominated by mafic minerals, including amphibole, and their bulk compositions are consistent with a cumulate origin. The origin of the xenoliths has been studied experimentally and using MELTS modelling, and interpreted as the progressive crystallisation sequence ol + sp, + cpx, + hbl, + plag, forming under hydrous conditions at 200-500 MPa, and with relatively small variations in host melt chemistry and temperature. The existence of robust independent experimental and modelling results for these cumulate rocks (Stamper et al. 2014) gives us a valuable opportunity to evaluate the applicability of our chemometric equations to plutonic amphiboles. Amphiboles are abundant in the majority of the xenoliths and in the andesitic host lavas, and most of the major element analyses indicate MgHst compositions, with occasional presence of Tsch and Parg (Stamper et al. 2014). Texturally, amphiboles in the xenoliths are present either as poikilitic interstitial crystals with inclusions of olivine, clinopyroxene, spinel and plagioclase, or as euhedral and equant crystals. Both types of amphiboles can be found in the amphibole-bearing cumulate nodules and lavas. To quantify the melt compositions that were in equilibrium with the cumulate crystals, we used published amphibole analyses from the xenoliths studied by Stamper et al. (2014) and calculated their corresponding melt compositions. The samples include clinopyroxenites (GRN17, GRN24, GR17, GR29, GR5-1),

hornblendites (GR15, GR25, GR11, GR52), hornblende gabbro (GRN6, GRN 21, GRN5), as well as one non-cumulate hornblende gabbro (GR42). The results are all included in the Appendix Table 1.

Although the ranges are overlapping, the results show a general trend of increasing calculated melt SiO_2 contents from the more evolved cumulates, with the non-cumulate gabbro yielding the highest melt SiO_2 (Fig. 9a). Amphiboles in clinopyroxenite give calculated melts with 52-60 wt% SiO_2 and 2.2-6.1 wt% MgO; amphiboles from the hornblendites give calculated melts with 52.9-62.6 wt% SiO_2 and 1.5-7.0 wt% MgO; amphiboles from the cumulate gabbros give calculated melts with 54.3-63.1 wt% SiO_2 and 1.8-4.3 wt% MgO; and the non-cumulate gabbro gives calculated melts with 58.1-70.8 wt% SiO_2 and 0.6-2.9 wt% MgO (Fig. 9f). Each individual sample occupies a part of these overall arrays. As with Ongatiti, the extent of any possible diffusive re-equilibration is probably small because Fe-Mg interdiffusion modelling results, displayed as vectors in Fig. 8, are inconsistent with variation trends of the predicted melt Al_2O_3 and FeO compositions. In comparison with melts calculated using the formulations of Ridolfi and Renzulli (2012), our compositions span a similar range of SiO_2 but with significantly higher and less scattered CaO (Fig. 9g), and slightly lower FeO (Fig. 9e). Inferred MgO concentrations cannot be compared easily due to the use of the pressure term for RR2012, which performs poorly (see Stamper et al. 2014 and Fig. 9f). This emphasises the advantage of our study in using pressure-independent (and temperature-independent) equations for melt chemistry. For TiO_2, the majority of the melts calculated using RR2012 fall on a steeper gradient with respect to SiO_2, compared with those calculated using our equations (Fig. 9c). Some of our calculated melts are offset to higher TiO_2; this is a result of slight differences in TiO_2 concentration in the raw amphibole analyses. A larger subset of the melts calculated using RR2012 have

475 similarly high TiO_2, but these are not obviously linked to any compositional signature except
476 those amphiboles with lower SiO_2 (Fig. 9c).

477 In general, the calculated melt compositions are also broadly in agreement with the
478 (strongly scattered) compositions of clinopyroxene-hosted melt inclusions measured by
479 Stamper et al. (2014) (Fig. 9). In particular, the melts inferred from amphibole in the non-
480 cumulate hornblende gabbro agree very well with the most evolved pyroxene-hosted melt
481 inclusion, from a (different) non-cumulate gabbro (Stamper et al. 2014; Fig. 9b-h). The
482 predicted melt compositions are also similar to the compositions of C-series lavas, and
483 consistent with low-pressure fractionation trend derived from MELTS modelling (Stamper *et*
484 *al.*, 2014; see Fig. 22 therein; Fig. 9b). These observations all indicate that our chemometric
485 equations are able to make reliable predictions of melt chemistry from amphibole major
486 element compositions.

487 Our predicted MgO concentrations project back towards the parental melts required to
488 form the clinopyroxenite - hornblendite - hornblende gabbro assemblages (Fig. 9f; i.e. 47.5-
489 51.3 wt % SiO_2 and 4.4-9.7 wt % MgO based on previous experimental studies, Stamper et al.
490 2014). These source melts are more mafic than our predicted melt compositions and the
491 majority of the measured melt inclusions hosted in cumulate mineral phases (Stamper *et al.*,
492 2014). We propose two possible reasons to explain this offset as follows. Firstly, the large
493 spread in our predicted melt compositions, and the melt inclusions, may reflect in situ melt
494 evolution during protracted crystallization of the cumulate mineral phases. This progressive
495 in situ fractionation can result in continuous and progressive changes to the residual
496 interstitial melt hosted in the cumulate, and therefore formation of new interstitial phases and
497 strongly zoned mineral overgrowths. Chemometric inversions using those zoned minerals
498 would predict an array of melt compositions for each sample, as observed in our dataset.
499 Unfortunately, there is insufficient detail about the textural locations of each amphibole

analysis from Stamper et al. (2014) to test this rigorously. Secondly, the appearance of mineral phases in the plutonic xenoliths follows the sequence olivine, clinopyroxene, amphibole and plagioclase with decreasing temperature (Stamper et al. 2014). In contrast, our chemometric equations can only predict melt compositions that coexisted with amphibole, so we invariably miss an early part of this liquid line of descent. We would therefore expect the most primitive melts, i.e., those present during formation of the wehrlite cumulates and those from the earlier stages of formation of the clinopyroxenite and hornblendite cumulates, to be absent from our results. However, overall our results indicate the differentiation of mafic to intermediate magmas within the crust under Grenada.

ACKNOWLEDGEMENTS

This work forms part of the first author's PhD research, which was funded by a Durham Doctoral Studentship (Durham University) and China Scholarship Council (201206170178). Madeleine Humphreys was supported by a Royal Society University Research Fellowship. George Cooper was supported by a NERC Postdoctoral Fellowship. We thank Kate Saunders and Yaoling Niu for their comments on an earlier version of this manuscript, and Adam Kent for useful discussions. We also acknowledge helpful journal reviews from Saskia Erdmann, Mike Rowe and an anonymous reviewer, and editorial assistance from Georg Zellmer.

REFERENCES

Adam, J., and Green, T. (2006). Trace element partitioning between mica- and amphibole-bearing garnet lherzolite and hydrous basanitic melt: 1. Experimental results and the investigation of controls on partitioning behaviour. Contributions to Mineralogy and Petrology, 152, 1-17.

523 Adam, J., and Green, T.H. (1994). The Effects of Pressure and Temperature on the
524 Partitioning of Ti, Sr and REE between Amphibole, Clinopyroxene and Basanitic
525 Melts. Chemical Geology, 117, 219-233.
526 Adam, J., Green, T.H., and Sie, S.H. (1993). Proton Microprobe Determined Partitioning of
527 Rb, Sr, Ba, Y, Zr, Nb and Ta between Experimentally Produced Amphiboles and
528 Silicate Melts with Variable F Content. Chemical Geology, 109, 29-49.
529 Allan, A.S.R., Morgan, D.J., Wilson, C.J.N ., and Millet, M. (2013). From mush to eruption
530 in centuries: assembly of the super-sized Oruanui magma body. Contributions to
531 Mineralogy and Petrology, 166, 143-164.
532 Alonso-Perez, R., Muntener, O., and Ulmer, P. (2009). Igneous garnet and amphibole
533 fractionation in the roots of island arcs: experimental constraints on andesitic liquids.
534 Contributions to Mineralogy and Petrology, 157, 541-558.
535 Anderson, J.L., and Smith, D.R. (1995). The Effects of Temperature and f(O_2) on the Al-in-
536 Hornblende Barometer. American Mineralogist, 80, 549-559.
537 Arculus, R.J., and Wills, K.J.A. (1980). The Petrology of Plutonic Blocks and Inclusions
538 from the Lesser Antilles Island Arc. Journal of Petrology, 21, 743-799.
539 Barclay, J., and Carmichael, I.S.E. (2004). A hornblende basalt from western Mexico: Water-
540 saturated phase relations constrain a pressure-temperature window of eruptibility.
541 Journal of Petrology, 45, 485-506.
542 Blatter, D.L., and Carmichael, I.S.E. (2001). Hydrous phase equilibria of a Mexican high-
543 silica andesite: A candidate for a mantle origin? Geochimica et Cosmochimica Acta,
544 65, 4043-4065.
545 Blundy, J., and Cashman, K. (2008). Petrologic Reconstruction of Magmatic System
546 Variables and Processes. Reviews in Mineralogy and Geochemistry, 69, 179-239.

547 Blundy, J.D., and Holland, T.J.B. (1990). Calcic Amphibole Equilibria and a New
548 Amphibole-Plagioclase Geothermometer. Contributions to Mineralogy and Petrology,
549 104, 208-224.
550 Bogaerts, M., Scaillet, B., and Auwera, J. V. (2006). Phase equilibria of the lyngdal
551 granodiorite (Norway): Implications for the origin of metaluminous ferroan granitolds.
552 Journal of Petrology, 47, 2405-2431.
553 Carroll, M.R., and Wyllie, P.J. (1989). Experimental Phase-Relations in the System Tonalite-
554 Peridotite-H2o at 15 Kb - Implications for Assimilation and Differentiation Processes
555 near the Crust-Mantle Boundary. Journal of Petrology, 30, 1351-1382.
556 Cashman, K., and Blundy, J. (2013). Petrological cannibalism: the chemical and textural
557 consequences of incremental magma body growth. Contributions to Mineralogy and
558 Petrology, 166, 703-729.
559 Chakraborty, S. (1997). Rates and mechanisms of Fe-Mg interdiffusion in olivine at 980º-
560 1300ºC. Journal of Geophysical Research-Solid Earth, 102, 12317-12331.
561 Cooper, G.F., and Wilson, C.J.N. (2014). Development, mobilisation and eruption of a large
562 crystal-rich rhyolite: The Ongatiti ignimbrite, New Zealand. Lithos, 198, 38-57.
563 Costa, F., Scaillet, B., and Pichavant, M. (2004). Petrological and experimental constraints on
564 the pre-eruption conditions of Holocene dacite from Volcan San Pedro (36°S, Chilean
565 Andes) and the importance of sulphur in silicic subduction-related magmas. Journal of
566 Petrology, 45, 855-881.
567 Dalpé, C., and Baker, D.R. (2000). Experimental investigation of large-ion-lithophile-
568 element-, high-field-strength-element- and rare-earth-element-partitioning between
569 calcic amphibole and basaltic melt: the effects of pressure and oxygen fugacity.
570 Contributions to Mineralogy and Petrology, 140, 233-250.

571 Davidson, J., Turner, S., Handley, H., Macpherson, C., and Dosseto, A. (2007). Amphibole
572 "sponge" in arc crust? Geology, 35, 787-790.
573 Erdmann, S., Martel, C., Pichavant, M., and Kushnir, A. (2014). Amphibole as an archivist of
574 magmatic crystallization conditions: problems, potential, and implications for
575 inferring magma storage prior to the paroxysmal 2010 eruption of Mount Merapi,
576 Indonesia. Contributions to Mineralogy and Petrology, 167, 1-23.
577 Ernst, W.G., and Liu, J. (1998). Experimental phase-equilibrium study of Al- and Ti-contents
578 of calcic amphibole in MORB - A semiquantitative thermobarometer. American
579 Mineralogist, 83, 952-969.
580 Fujinawa, A., and Green, T.H. (1997). Experimental study of partitioning of Hf and Zr
581 between amphibole, clinopyroxene, garnet, and silicate melts. Journal of Mineralogy
582 Petrology and Economic Geology, 2, 69-89 (in Japanese).
583 Gardner, J.E., Rutherford, M., Carey, S., and Sigurdsson, H. (1995). Experimental
584 Constraints on Pre-Eruptive Water Contents and Changing Magma Storage Prior to
585 Explosive Eruptions of Mount St-Helens Volcano. Bulletin of Volcanology, 57, 1-17.
586 Green, T.H., and Pearson, N.J. (1985). Experimental-Determination of Ree Partition-
587 Coefficients between Amphibole and Basaltic to Andesitic Liquids at High-Pressure.
588 Geochimica et Cosmochimica Acta, 49, 1465-1468.
589 Grove, T.L., DonnellyNolan, J.M., and Housh, T. (1997). Magmatic processes that generated
590 the rhyolite of Glass Mountain, Medicine Lake volcano, N California. Contributions
591 to Mineralogy and Petrology, 127, 205-223.
592 Grove, T.L., Elkins-Tanton, L.T., Parman, S.W., Chatterjee, N., Muntener, O., and Gaetani,
593 G.A. (2003). Fractional crystallization and mantle-melting controls on calc-alkaline
594 differentiation trends. Contributions to Mineralogy and Petrology, 145, 515-533.

595 Hammarstrom, J.M., and Zen, E.A. (1986). Aluminum in Hornblende: an Empirical Igneous
596 Geobarometer. American Mineralogist, 71, 1297-1313.
597 Hawthorne, F.C., Oberti, R., Harlow, G.E., Maresch, W.V., Martin, R.F., Schumacher, J.C.,
598 and Welch, M.D. (2012). Nomenclature of the amphibole supergroup. American
599 Mineralogist, 97, 2031-2048.
600 Hilyard, M., Nielsen, R.L., Beard, J.S., Patino-Douce, A., and Blencoe, J. (2000).
601 Experimental determination of the partitioning behavior of rare earth and high field
602 strength elements between pargasitic amphibole and natural silicate melts.
603 Geochimica et Cosmochimica Acta, 64, 1103-1120.
604 Hirschmann, M.M., Ghiorso, M.S., Davis, F.A., Gordon, S.M., Mukherjee, S., Grove, T.L.,
605 Krawczynski, M., Medard, E., and Till, C.B. (2008). Library of Experimental Phase
606 Relations (LEPR): A database and Web portal for experimental magmatic phase
607 equilibria data. Geochemistry, Geophysics, Geosystems, 9, 1711-1730.
608 Holland, T., and Blundy, J. (1994). Nonideal Interactions in Calcic Amphiboles and Their
609 Bearing on Amphibole-Plagioclase Thermometry. Contributions to Mineralogy and
610 Petrology, 116, 433-447.
611 Hollister, L.S., Grissom, G.C., Peters, E.K., Stowell, H.H., and Sisson, V.B. (1987).
612 Confirmation of the Empirical Correlation of Al in Hornblende with Pressure of
613 Solidification of Calc-Alkaline Plutons. American Mineralogist, 72, 231-239.
614 Holtz, F., Sato, H., Lewis, J., Behrens, H., and Nakada, S. (2005). Experimental petrology of
615 the 1991-1995 Unzen dacite, Japan. Part I: Phase relations, phase composition and
616 pre-eruptive conditions. Journal of Petrology, 46, 319-337.
617 Houghton, B.F., Wilson, C.J.N., McWilliams, M.O., Lanphere, M.A., Weaver, S.D., Briggs,
618 R.M., and Pringle, M.S. (1995). Chronology and dynamics of a large silicic magmatic
619 system: central Taupo Volcanic Zone, New Zealand. Geology, 23, 13-16.

620 Huber, C., Bachmann, O., and Manga, M. (2009). Homogenization processes in silicic
621 magma chambers by stirring and mushification (latent heat buffering). Earth and
622 Planetary Science Letters, 283, 38-47.
623 Humphreys, M.C.S., Blundy, J.D., and Sparks, R.S.J. (2006a). Magma Evolution and Open-
624 System Processes at Shiveluch Volcano: Insights from Phenocryst Zoning. Journal of
625 Petrology, 47, 2303-2334.
626 Humphreys, M.C.S., Kearns, S.L., and Blundy, J.D. (2006b). SIMS investigation of electron-
627 beam damage to hydrous, rhyolitic glasses: Implications for melt inclusion analysis.
628 American Mineralogist, 91, 667-679.
629 Kawamoto, T. (1996). Experimental constraints on differentiation and H_2O abundance of
630 calc-alkaline magmas. Earth and Planetary Science Letters, 144, 577-589.
631 Klein, M., Stosch, H.G., and Seck, H.A. (1997). Partitioning of high field-strength and rare-
632 earth elements between amphibole and quartz-dioritic to tonalitic melts: An
633 experimental study. Chemical Geology, 138, 257-271.
634 Klugel, A. (2001). Prolonged reactions between harzburgite xenoliths and silica-
635 undersaturated melt: implications for dissolution and Fe-Mg interdiffusion rates of
636 orthopyroxene. Contributions to Mineralogy and Petrology, 141, 1-14.
637 Krawczynski, M.J., Grove, T.L., and Behrens, H. (2012). Amphibole stability in primitive arc
638 magmas: effects of temperature, H_2O content, and oxygen fugacity. Contributions to
639 Mineralogy and Petrology, 164, 317-339.
640 Leake, B.E., Woolley, A.R., Arps, C.E.S., Birch, W.D., Gilbert, M.C., Grice, J.D.,
641 Hawthorne, F.C., Kato, A., Kisch, H.J., Krivovichev, V.G., and others (1997).
642 Nomenclature of amphiboles: Report of the subcommittee on amphiboles of the
643 International Mineralogical Association, Commission on New Minerals and Mineral
644 Names. Canadian Mineralogist, 35, 219-246.

Martel, C., Champallier, R., Prouteau, G., Pichavant, M., Arbaret, L., Balcone-Boissard, H., Boudon, G., Boivin, P., Bourdier, J.L., and Scaillet, B. (2013). Trachyte Phase Relations and Implication for Magma Storage Conditions in the Chaine des Puys (French Massif Central). Journal of Petrology, 54, 1071-1107.

Molina, J.F., Moreno, J.A., Castro, A., Rodríguez, C., and Fershtater, G.B. (2015). Calcic amphibole thermobarometry in metamorphic and igneous rocks: New calibrations based on plagioclase/amphibole Al-Si partitioning and amphibole/liquid Mg partitioning. Lithos, 232, 286-305.

Moore, G., and Carmichael, I.S.E. (1998). The hydrous phase equilibria (to 3 kbar) of an andesite and basaltic andesite from western Mexico: constraints on water content and conditions of phenocryst growth. Contributions to Mineralogy and Petrology, 130, 304-319.

Muller, T., Dohmen, R., Becker, H.W., ter Heege, J.H., and Chakraborty, S. (2013). Fe-Mg interdiffusion rates in clinopyroxene: experimental data and implications for Fe-Mg exchange geothermometers. Contributions to Mineralogy and Petrology, 166, 1563-1576.

Nandedkar, R.H. (2014). Evolution of hydrous mantle-derived calc-alkaline liquids by fractional crystallization at 0.7 and 0.4 GPa – An experimental study. Ph.D. thesis, ETH.

Naney, M.T. (1983). Phase-Equilibria of Rock-Forming Ferromagnesian Silicates in Granitic Systems. American Journal of Science, 283, 993-1033.

Nekvasil, H., Dondolini, A., Horn, J., Filiberto, J., Long, H., and Lindsley, D.H. (2004). The origin and evolution of silica-saturated alkalic suites: an experimental study. Journal of Petrology, 45, 693-721.

669 Nicholls, I.A., and Harris, K.L. (1980). Experimental Rare-Earth Element Partition-
670 Coefficients for Garnet, Clinopyroxene and Amphibole Coexisting with Andesitic and
671 Basaltic Liquids. Geochimica et Cosmochimica Acta, 44, 287-308.
672 Patino-Douce, A.E., and Beard, J.S. (1995). Dehydration-Melting of Biotite Gneiss and
673 Quartz Amphibolite from 3 to 15 Kbar. Journal of Petrology, 36, 707-738.
674 Pichavant, M., Di Carlo, I., Le Gac, Y., Rotolo, S.G., and Scaillet, B. (2009). Experimental
675 Constraints on the Deep Magma Feeding System at Stromboli Volcano, Italy. Journal
676 of Petrology, 50, 601-624.
677 Pichavant, M., Martel, C., Bourdier, J.L., and Scaillet, B. (2002). Physical conditions,
678 structure, and dynamics of a zoned magma chamber: Mount Pelee (Martinique, Lesser
679 Antilles Arc). Journal of Geophysical Research, 107(B5), 1-26.
680 Prouteau, G., and Scaillet, B. (2003). Experimental constraints on the origin of the 1991
681 Pinatubo dacite. Journal of Petrology, 44, 2203-2241.
682 Prouteau, G., Scaillet, B., Pichavant, M., and Maury, R.C. (1999). Fluid-present melting of
683 ocean crust in subduction zones. Geology, 27, 1111-1114.
684 Putirka, K.A. (2016). Amphibole thermometers and barometers for igneous systems, and
685 some implications for eruption mechanism of felsic magmas at arc volcanoes.
686 American Mineralogist, 101, 841-858.
687 Putirka, K.D. (2008). Thermometers and Barometers for Volcanic Systems. Reviews in
688 Mineralogy and Geochemistry, 69, 61-120.
689 Reubi, O., and Blundy, J. (2009). A dearth of intermediate melts at subduction zone
690 volcanoes and the petrogenesis of arc andesites. Nature, 461, 1269-1273.
691 Ridolfi, F., Puerini, M., Renzulli, A., Menna, M., and Toulkeridis, T. (2008). The magmatic
692 feeding system of El Reventador volcano (Sub-Andean zone, Ecuador) constrained by

texture, mineralogy and thermobarometry of the 2002 erupted products. Journal of Volcanology and Geothermal Research, 176, 94-106.

Ridolfi, F., and Renzulli, A. (2012). Calcic amphiboles in calc-alkaline and alkaline magmas: thermobarometric and chemometric empirical equations valid up to 1,130°C and 2.2 GPa. Contributions to Mineralogy and Petrology, 163, 877-895.

Ridolfi, F., Renzulli, A., and Puerini, M. (2010). Stability and chemical equilibrium of amphibole in calc-alkaline magmas: an overview, new thermobarometric formulations and application to subduction-related volcanoes. Contributions to Mineralogy and Petrology, 160, 45-66.

Roeder, P.L., and Emslie, R.F. (1970). Olivine-Liquid Equilibrium. Contributions to Mineralogy and Petrology, 29, 275-289.

Rutherford, M.J., and Devine, J.D. (2003). Magmatic conditions and magma ascent as indicated by hornblende phase equilibria and reactions in the 1995-2002 Soufriere Hills magma. Journal of Petrology, 44, 1433-1454.

Sato, H., Holtz, F., Behrens, H., Botcharnikov, R., and Nakada, S. (2005). Experimental petrology of the 1991-1995 Unzen dacite, Japan. Part II: Cl/OH partitioning between hornblende and melt and its implications for the origin of oscillatory zoning of hornblende phenocrysts. Journal of Petrology, 46, 339-354.

Scaillet, B., and Evans, B.W. (1999). The 15 June 1991 eruption of Mount Pinatubo. I. Phase equilibria and pre-eruption P-T-fO_2-fH_2O conditions of the dacite magma. Journal of Petrology, 40, 381-411.

Schmidt, M.W. (1992). Amphibole Composition in Tonalite as a Function of Pressure: an Experimental Calibration of the Al-in-Hornblende Barometer. Contributions to Mineralogy and Petrology, 110, 304-310.

717 Shane, P., and Smith, V.C. (2013). Using amphibole crystals to reconstruct magma storage
718 temperatures and pressures for the post-caldera collapse volcanism at Okataina
719 volcano. Lithos, 156-159, 159-170.
720 Sisson, T.W. (1994). Hornblende-Melt Trace-Element Partitioning Measured by Ion
721 Microprobe. Chemical Geology, 117, 331-344.
722 Sisson, T.W., and Grove, T.L. (1993). Experimental Investigations of the Role of H2O in
723 Calc-Alkaline Differentiation and Subduction Zone Magmatism. Contributions to
724 Mineralogy and Petrology, 113, 143-166.
725 Skjerlie, K.P., and Johnston, A.D. (1996). Vapour-absent melting from 10 to 20 kbar of
726 crustal rocks that contain multiple hydrous phases: Implications for anatexis in the
727 deep to very deep continental crust and active continental margins. Journal of
728 Petrology, 37, 661-691.
729 Smith, D.J. (2014). Clinopyroxene precursors to amphibole sponge in arc crust. Nature
730 Communications, 5, 787.
731 Springer, W., and Seck, H.A. (1997). Partial fusion of basic granulites at 5 to 15 kbar:
732 Implications for the origin of TTG magmas. Contributions to Mineralogy and
733 Petrology, 127, 30-45.
734 Stamper, C.C., Blundy, J.D., Arculus, R.J., and Melekhova, E. (2014). Petrology of Plutonic
735 Xenoliths and Volcanic Rocks from Grenada, Lesser Antilles. Journal of Petrology,
736 55, 1353-1387.
737 Streck, M.J. (2008). Mineral Textures and Zoning as Evidence for Open System Processes.
738 Reviews in Mineralogy and Geochemistry, 69, 595-622.
739 Tiepolo, M., Vannucci, R., Bottazzi, P., Oberti, R., Zanetti, A., and Foley, S. (2000).
740 Partitioning of rare earth elements, Y, Th, U, and Pb between pargasite, kaersutite,

and basanite to trachyte melts: Implications for percolated and veined mantle. Geochemistry Geophysics Geosystems, 1, 20431-20450.

Zhang, J., Davidson, J.P., Humphreys, M.C.S., Macpherson, C.G., and Neill, I. (2015). Magmatic Enclaves and Andesitic Lavas from Mt. Lamington, Papua New Guinea: Implications for Recycling of Earlier-fractionated Minerals through Magma Recharge. Journal of Petrology, 56, 2223-2256.

FIGURE CAPTIONS

Fig. 1 (a-b) Experimental P-T run conditions, and (c-d) the relationship between temperature and melt SiO_2 content of the selected experiments. (a) and (c) illustrate the overlap in P-T-X conditions between the studies selected for calibrating chemometric equations and for testing the accuracy of the equations. (b) and (d) illustrate the corresponding amphibole species in terms of MgHst (magnesiohastingsite), MgHbl (magnesiohornblende), Parg (pargasite), Tsch (tschermakite) and Kaer (kaersutite), as well as amphiboles which are either non-calcic or have compositions out of equilibrium with the melt. The area outlined in (b) denotes the P-T window within which calcic amphiboles can crystallize and equilibrate with the melt. The arrow in (d) outlines the approximate liquid line of descent. (e-f) The relationships between amphibole crystal chemistry (Si_T, in apfu) and temperature and melt SiO_2 content (normalized to 100% anhydrous). See text for details.

Fig. 2 Calcic amphibole formula proportions of Parg, MgHst, Kaer, Tsch and MgHbl from the selected experimental studies. Symbols as for figure 1b, d.

Fig. 3 Test for equilibrium between amphibole and melt based on the Fe-Mg exchange coefficient (K_D). The amphibole and melt compositions are regarded as in

763 equilibrium when K_D is within the range of 0.28 ± 0.11 (Putirka 2016). Symbols as for figure
764 1a, c.

765 Fig. 4 Major element compositions of melts from the selected experimental studies
766 (normalized to 100% anhydrous). Symbols as for figure 1b, d.

767 Fig. 5 (a) Predicted melt MgO using Ridolfi and Renzulli (2012)'s model vs.
768 measured MgO; (b) the overestimation of melt MgO at > 3 wt % is strongly dependent on the
769 pressure (> 1,000 MPa) calculated with Ridolfi and Renzulli (2012)'s barometer model.
770 Symbols as for figure 1b, d.

771 Fig. 6 Comparison between experimental and predicted melt compositions for the
772 calibration group (blue) and test group (red) using equations from Table 1, and results
773 calculated using Ridolfi and Renzulli (2012)'s chemometric equations (open circles). The
774 multiple regression analysis can reproduce the melt major element compositions with better
775 accuracy than Ridolfi and Renzulli (2012)'s model, which can generate a large offset from
776 measured melt compositions especially in the low-SiO_2 group and for TiO_2, FeO, MgO, CaO
777 and K_2O. Correlation coefficients and standard error of estimates are given in each plot for
778 the calibration results (R^2 and *SE*) and test results (r^2 and *se*). See text for details.

779 Fig. 7 Back-scattered electron SEM images of amphibole crystals from the Ongatiti
780 ignimbrite. (a) Type A crystal with non-distinct core and finely oscillatory zoned rim (no
781 compositional contrast). (b-c) Type B crystals with patchy zoned core (brighter patches of
782 MgHbl compositions and dark patches of MgHst compositions) and finely oscillatory zoned
783 rim (MgHbl), and with the presence of apatite and Fe-Ti oxides inclusions. The crystal in
784 panel (c) has a more distinct core-rim boundary than the crystal in panel (b).

Fig. 8 Melt compositions predicted from cores and rims of amphiboles in the Ongatiti ignimbrite, and the measured compositions of coexisting matrix glasses of pumice clasts (Cooper et al., 2014). The two vectors shown in each panel illustrate the effect of arbitrarily changing the Mg# of two representative amphiboles (a MgHst with Mg# of 0.67, and a MgHbl with Mg# of 0.57) as a result of Fe-Mg interdiffusion in modifying the predicted melt compositions; small black symbols represent increments of 0.10 in Mg# as labelled in panel *a* (see text for details). Panel (d) shows that the predicted MgO and SiO_2 in melts in equilibrium with amphiboles in the Ongatiti ignimbrite fall into the field of compositional array of global melt inclusions from Reubi and Blundy (2009).

Fig. 9 (a) Melt compositions inferred from amphibole in clinopyroxenite, hornblendite and hornblende gabbro cumulate xenoliths from Grenada, as well as non-cumulate hornblende gabbro (data from Stamper et al. 2014). Curves in (b) illustrate the results of MELTS modelling with a range of pressure input (from Stamper et al. 2014). The variations of the predicted melt CaO content and MgO content are consistent with low- to moderate-pressure fractionation. As with melt prediction results of Ongatiti amphiboles, the predicted MgO and SiO_2 in melts in equilibrium with amphiboles in Grenada cumulates and the non-cumulate gabbro also plot within the compositional array of global melt inclusions (Reubi and Blundy 2009). Panel (f) also illustrates that the predicted melt MgO and SiO_2 compositions project back towards initial melts parental to clinopyroxenite/hornblendite (open square) and hornblende gabbro (open circle), inferred from earlier experimental studies (Stamper et al. 2014). The melt compositions predicted using Ridolfi and Renzulli (2012)'s model are plotted as areas outlined in dotted lines. See further discussion in the text.

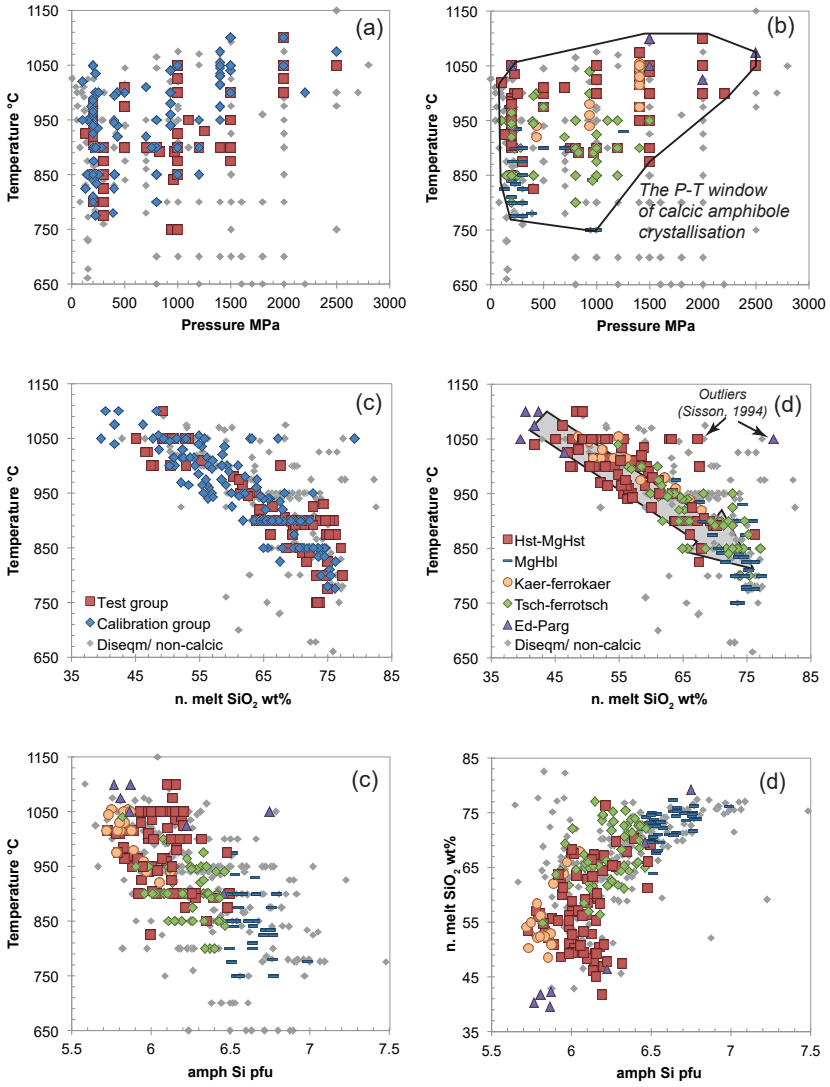
(a)
(b)
(c)
(d)
Temperature °C
Pressure MPa
The P-T window
of calcic amphibole
crystallisation
Outliers
(Sisson, 1994)
Test group
Calibration group
Diseqm/ non-calcic
Hst-MgHst
MgHbl
Kaer-ferrokaer
Tsch-ferrotsch
Ed-Parg
n. melt SiO2 wt%
amph Si pfu

Figure 1

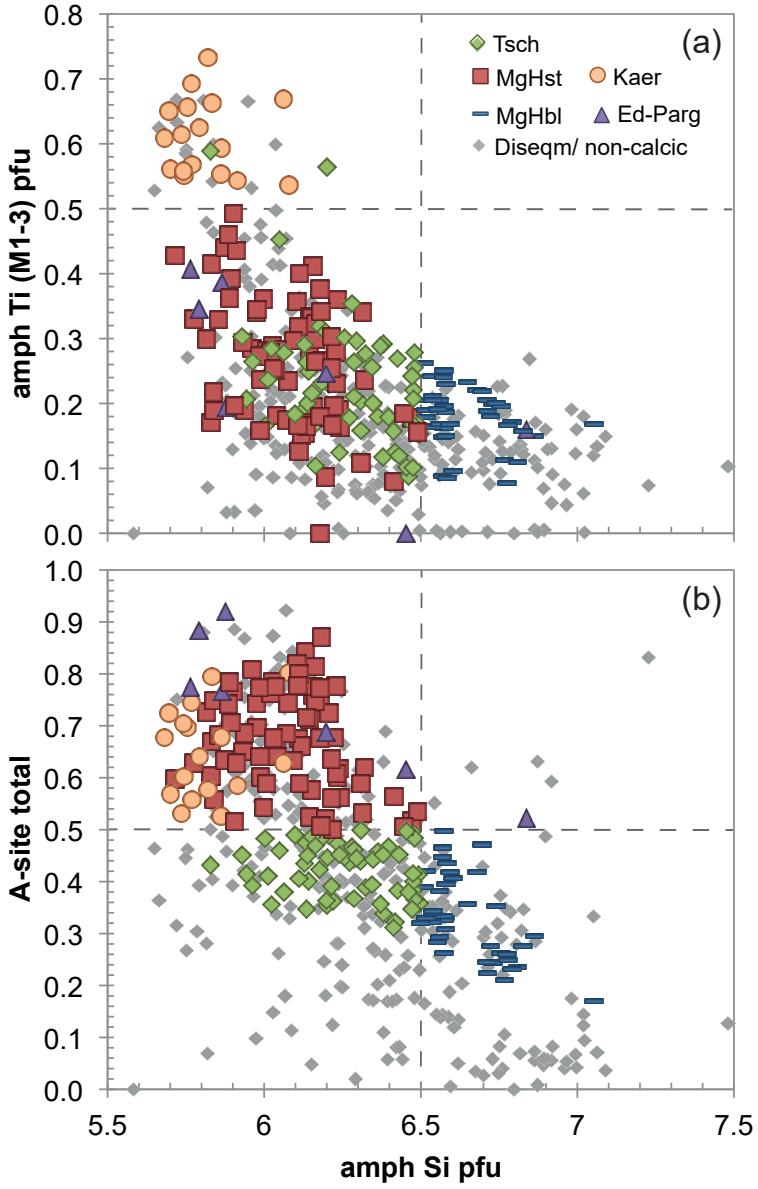
(a)
Tsch
MgHst
Kaer
MgHbl
Ed-Parg
Diseqm/ non-calcic
amph Ti (M1-3) pfu
0.0
0.1
0.2
0.3
0.4
0.5
0.6
0.7
0.8
(b)
A-site total
0.0
0.1
0.2
0.3
0.4
0.5
0.6
0.7
0.8
0.9
1.0
5.5
6
6.5
7
7.5
amph Si pfu

Figure 2

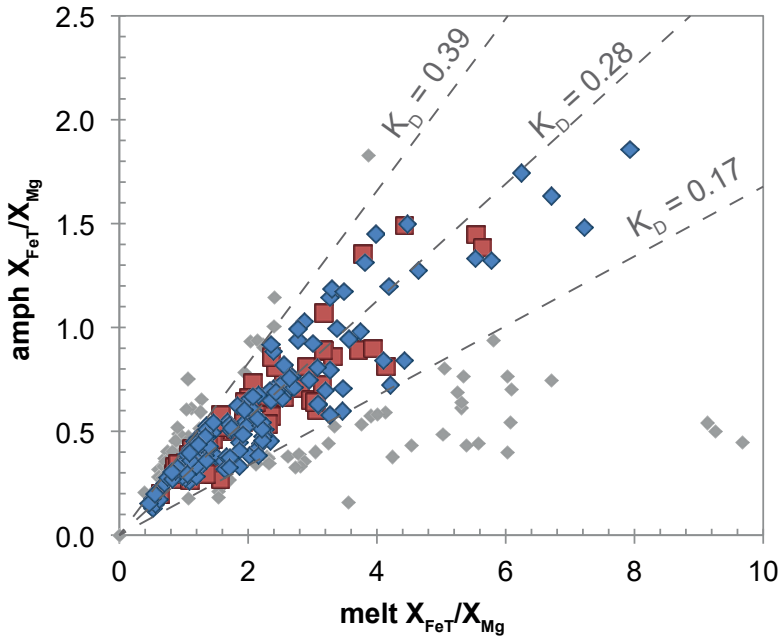
2.5
2.0
1.5
1.0
0.5
0.0
0
2
4
6
8
10
amph X_{FeT}/X_{Mg}
melt X_{FeT}/X_{Mg}
$K_D = 0.39$
$K_D = 0.28$
$K_D = 0.17$

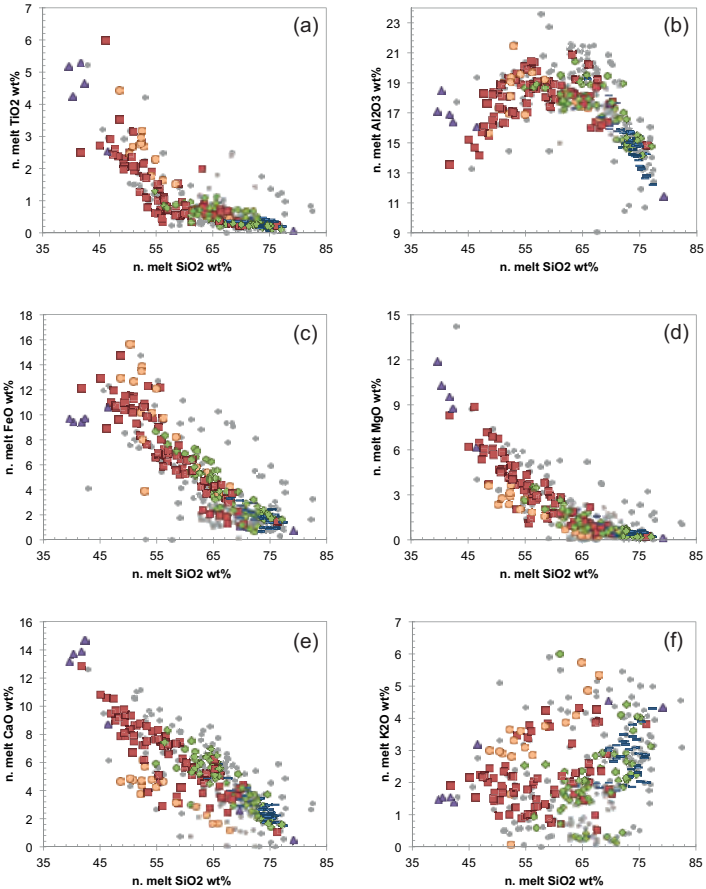
(a)
n. melt TiO2 wt%
n. melt SiO2 wt%
(b)
n. melt Al2O3 wt%
n. melt SiO2 wt%
(c)
n. melt FeO wt%
n. melt SiO2 wt%
(d)
n. melt MgO wt%
n. melt SiO2 wt%
(e)
n. melt CaO wt%
n. melt SiO2 wt%
(f)
n. melt K2O wt%
n. melt SiO2 wt%

Figure 4

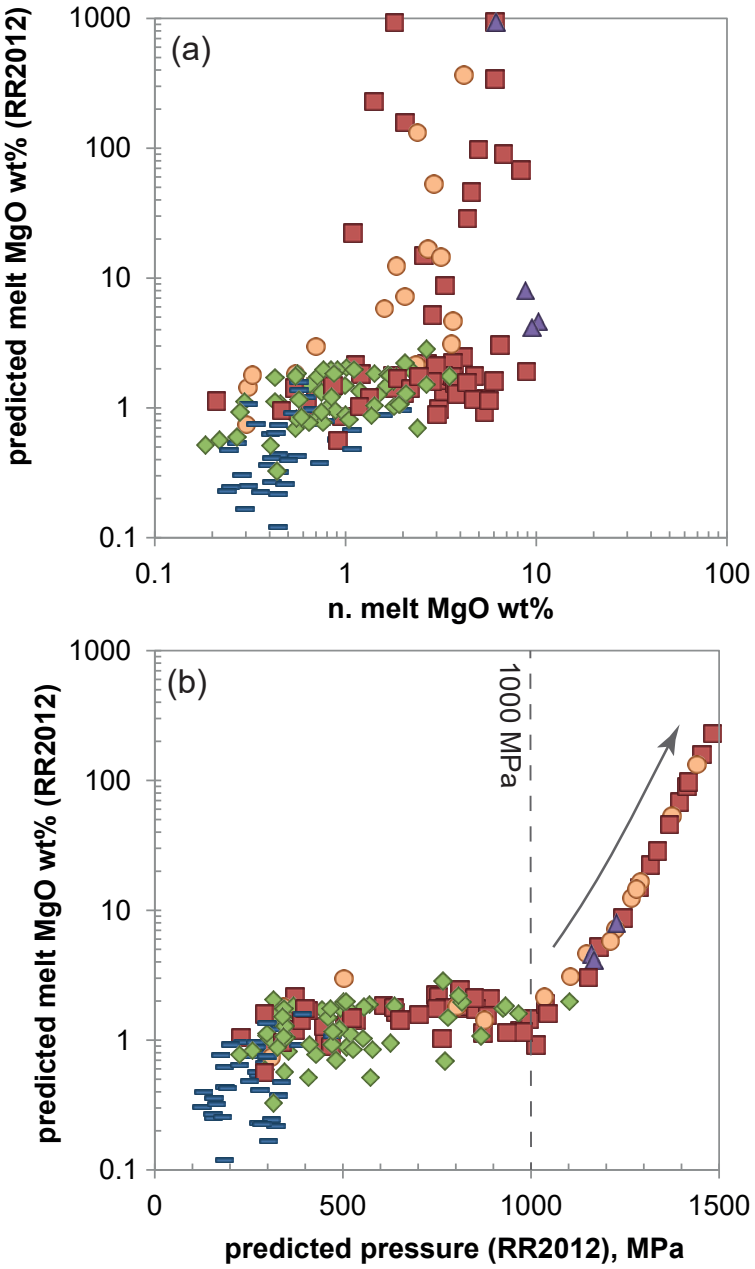
(a)
predicted melt MgO wt% (RR2012)
n. melt MgO wt%
1000
100
10
1
0.1
0.1
1
10
100
(b)
1000 MPa
predicted melt MgO wt% (RR2012)
predicted pressure (RR2012), MPa
0
500
1000
1500

Figure 5

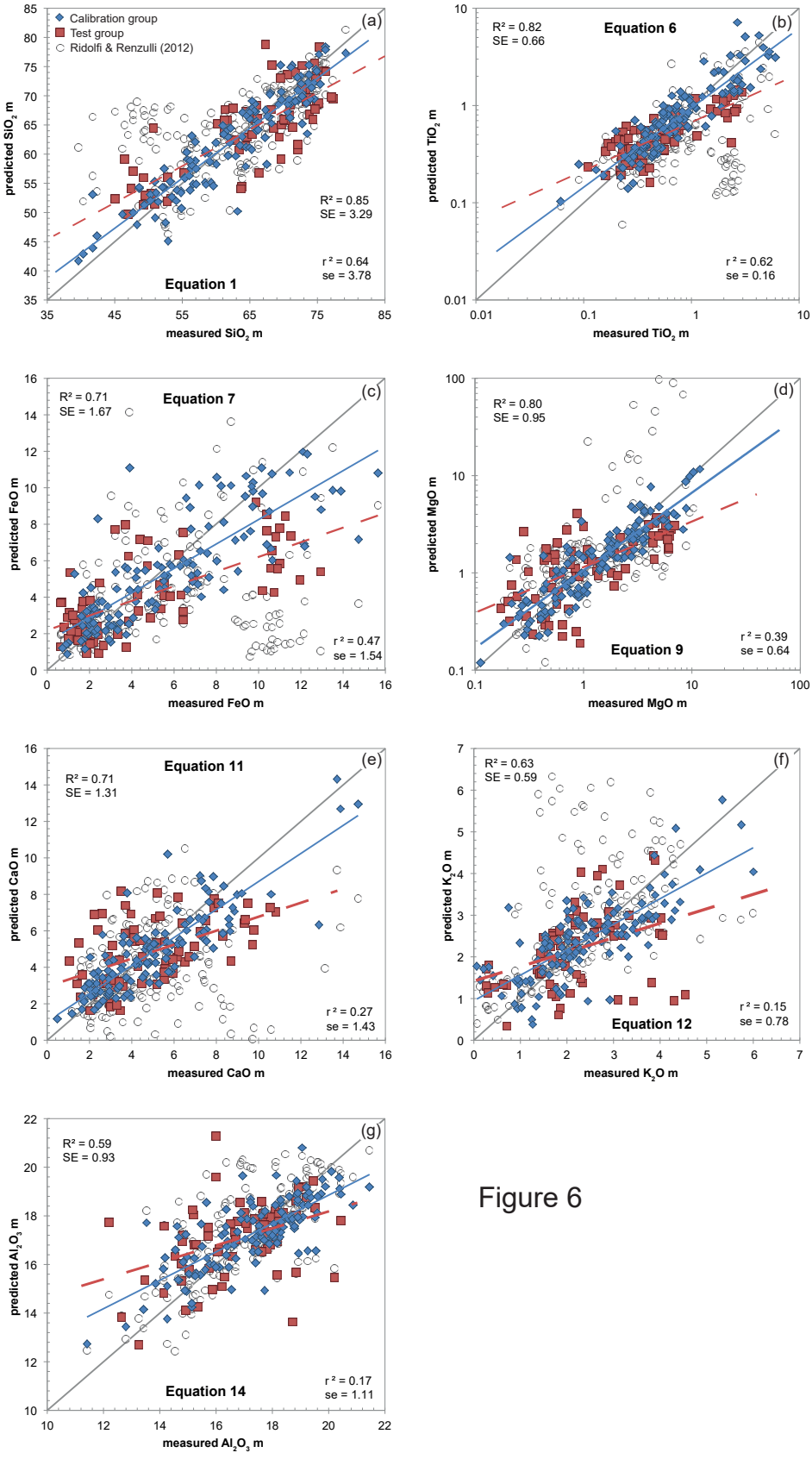
Calibration group
Test group
Ridolfi & Renzulli (2012)
(a)
predicted SiO2 m
measured SiO2 m
R² = 0.85
SE = 3.29
r ² = 0.64
se = 3.78
Equation 1
(b)
R² = 0.82
SE = 0.66
Equation 6
predicted TiO2 m
measured TiO2 m
r ² = 0.62
se = 0.16
(c)
R² = 0.71
SE = 1.67
Equation 7
predicted FeO m
measured FeO m
r ² = 0.47
se = 1.54
(d)
R² = 0.80
SE = 0.95
predicted MgO m
measured MgO m
Equation 9
r ² = 0.39
se = 0.64
(e)
Equation 11
R² = 0.71
SE = 1.31
predicted CaO m
measured CaO m
r ² = 0.27
se = 1.43
(f)
R² = 0.63
SE = 0.59
predicted K2O m
measured K2O m
Equation 12
r ² = 0.15
se = 0.78
(g)
R² = 0.59
SE = 0.93
predicted Al2O3 m
measured Al2O3 m
Equation 14
r ² = 0.17
se = 1.11

Figure 6

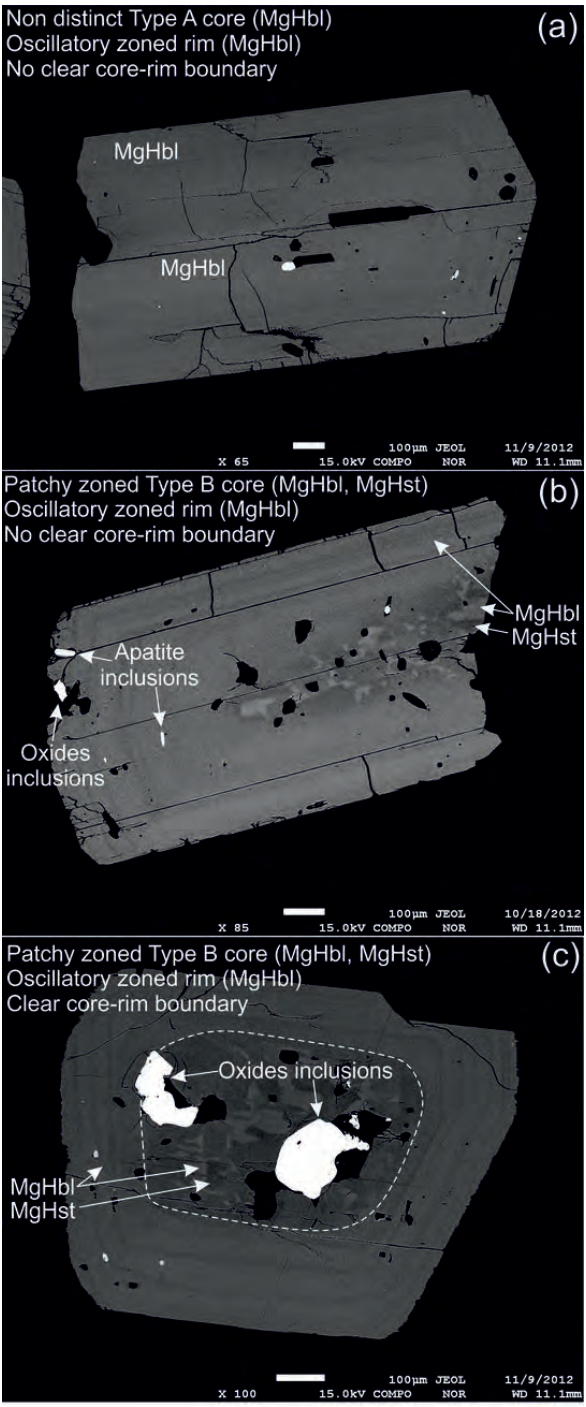
Non distinct Type A core (MgHbl)
Oscillatory zoned rim (MgHbl)
No clear core-rim boundary
(a)
MgHbl
MgHbl
X 65 15.0kV COMPO NOR 100µm JEOL WD 11.1mm 11/9/2012
Patchy zoned Type B core (MgHbl, MgHst)
Oscillatory zoned rim (MgHbl)
No clear core-rim boundary
(b)
MgHbl
MgHst
Apatite inclusions
Oxides inclusions
X 85 15.0kV COMPO NOR 100µm JEOL WD 11.1mm 10/18/2012
Patchy zoned Type B core (MgHbl, MgHst)
Oscillatory zoned rim (MgHbl)
Clear core-rim boundary
(c)
Oxides inclusions
MgHbl
MgHst
X 100 15.0kV COMPO NOR 100µm JEOL WD 11.1mm 11/9/2012

Figure 7

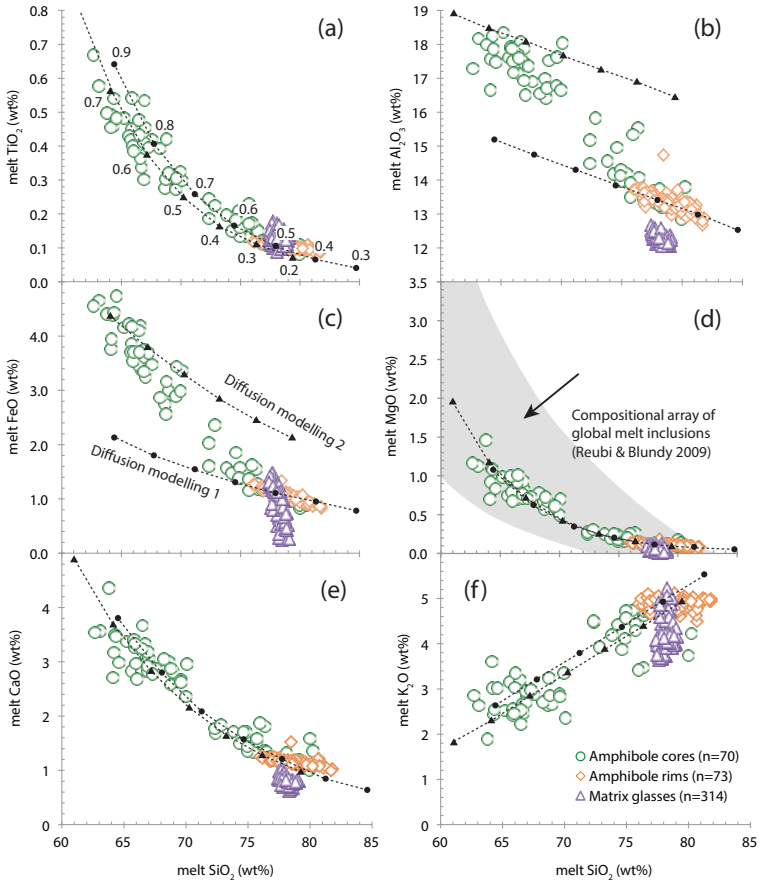
(a)
(b)
(c)
(d)
(e)
(f)
melt TiO2 (wt%)
melt Al2O3 (wt%)
melt FeO (wt%)
melt MgO (wt%)
melt CaO (wt%)
melt K2O (wt%)
melt SiO2 (wt%)
Diffusion modelling 2
Diffusion modelling 1
Compositional array of
global melt inclusions
(Reubi & Blundy 2009)
Amphibole cores (n=70)
Amphibole rims (n=73)
Matrix glasses (n=314)

Figure 8 new

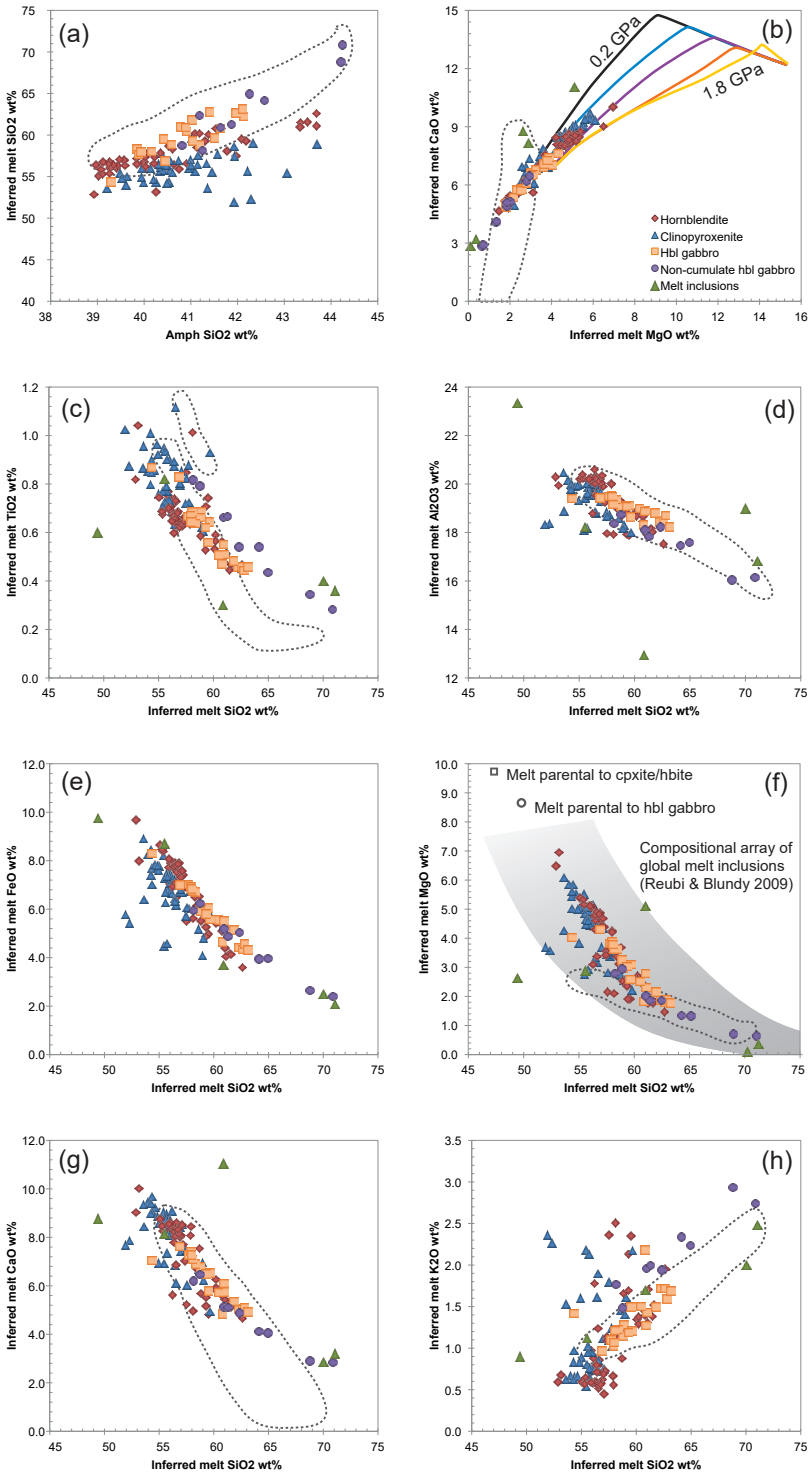
(a)
Inferred melt SiO2 wt%
Amph SiO2 wt%
(b)
0.2 GPa
1.8 GPa
Inferred melt CaO wt%
Inferred melt MgO wt%
Hornblendite
Clinopyroxenite
Hbl gabbro
Non-cumulate hbl gabbro
Melt inclusions
(c)
Inferred melt TiO2 wt%
Inferred melt SiO2 wt%
(d)
Inferred melt Al2O3 wt%
Inferred melt SiO2 wt%
(e)
Inferred melt FeO wt%
Inferred melt SiO2 wt%
(f)
Melt parental to cpxite/hbite
Melt parental to hbl gabbro
Compositional array of global melt inclusions (Reubi & Blundy 2009)
Inferred melt MgO wt%
Inferred melt SiO2 wt%
(g)
Inferred melt CaO wt%
Inferred melt SiO2 wt%
(h)
Inferred melt K2O wt%
Inferred melt SiO2 wt%

Figure 9

Table 1 Materials, conditions and run products of the selected experimental studies

References for calibration	Rock type	*N* (130)	*P* MPa	*T* ºC
Adam & Green 1994	basanite	5	500-2,000	1,000-1,100
Alonso-Perez et al., 2009	andesite	12	800-1,200	800-950
Barclay & Carmichael 2004	trachybasalt	3	104-223	1000-1035
Bogaerts et al. 2006	granodiorite	2	404	850
Costa et al. 2004	dacite	4	200-206	850-900
Dalpé & Baker, 2000	basanite-basalt	7	1,500-2,500	1,000-1,100
Gardner et al., 1995	dacite	6	150-250	850
Green & Pearson 1985	andesite	4	750-2,000	900-1,050
Grove et al. 2003	Mg andesite	1	200	990
Hilyard et al. 2000	dacite-tonalite	5	200-500	900-945
Klein et al. 1997	dacite	2	1,000	850-900
Martel et al. 2013	trachyte	2	200-400	825-900
Moore & Carmichael, 1998	basaltic andesite-andesite	6	101-250	900-1,000
Nandedkar 2014	basaltic andesite-rhyolite	3	700	920-1,010
Nekvasil et al., 2004	basalt-dacite	8	430-930	920-1040
Nicholls & Harris 1980	basalt-andesite	1	1,000	900
Pichavant et al. 2002	basaltic andesite	6	399-427	945-1,000
Pichavant et al. 2009	quartz diorite	3	200	850
Rutherford & Devine 2003	andesite	3	200	810-840
Sato et al. 2005	dacite	5	200	850
Scaillet & Evans 1999	dacite	7	224-389	776-899
Sisson 1994	basalt-andesite-dacite	4	200	1050
Sisson & Grove 1993	high-Al basalt	11	200	925-970
Tiepolo et al. 2000	basalt-andesite	20	1400	950-1075
Overall dataset contains 43 Hst-MgHst, 39 Tsch, 17 Kaer-Ferrokaersutite, 24 MgHbl-ferrohornblende, and 5 Edenite-				

References for test	Rock type	*N* (74)	*P* MPa	*T* ºC
Adam & Green 2006	basanite	1	1,000	1,025
Adam et al. 1993	basanite-basalt	4	1,000-2,000	1,000-1,050
Blatter & Carmichael, 2001	andesite	2	132-194	925-950
Carroll & Wyllie, 1989	tonalite	2	1,500	900-950
Ernst & Liu, 1998	basalt	5	800-1,400	900-950
Fujinawa & Green, 1997	basalt-andesite	16	500-2,000	900-1,100
Grove et al., 1997	basalt	5	200	905-980
Holtz et al., 2005	dacite	10	200-300	775-875
Kawamoto, 1996	basaltic andesite	2	500	975
Naney, 1983	granodiorite	2	800	900
Patino-Douce & Beard, 1995	quartz amphibolite	6	300-1,250	875-930
Prouteau & Scaillet, 2003	dacite	9	830-970	750-892
Prouteau et al., 1999	dacite	2	220-1,000	750-899
Skjerlie & Johnston, 1996	andesitic metavolcanoclastics	4	1,000-1,500	850-900
Springer & Seck, 1997	granulite	2	1,000-1,500	900-1,000
Overall dataset contains 30 MgHst, 21 Tsch, 2 Prg, 18 MgHbl and 1 Ferrohornblende (n = 72). Melt compositional rar				

Y indicates the data of the reference are also used in the calibrations of chemometric equations in Ridolfi & Renzulli (

Amphibole Species	RR2012	E2014
MgHst	Y	
Tsch		
MgHst		Y
Tsch		Y
MgHbl, MgHst	Y	Y
MgHst, Parg	Y	
Tsch, MgHbl	Y	
MgHst, Parg, Tsch		
MgHst		
MgHst, MgHbl, Parg, Tsch		
Tsch		
MgHst		Y
MgHbl, Tsch	Y	
Tsch, MgHst		
Kaer, Tsch	Y	
Tsch		
Tsch	Y	Y
MgHst, Tsch		
MgHbl	Y	Y
MgHbl, Tsch	Y	Y
MgHbl, Tsch	Y	Y
MgHbl, MgHst		
MgHst		Y
Kaer, MgHst, Parg		

Prg (n = 128). Melt compositional range 39.6 - 79.9 wt% SiO2 and 0.1 - 11.9 wt% MgO.

Amphibole Species	RR2012	E2014
MgHst		
MgHst, Parg		
Tsch		
MgHst, Parg		
Tsch		
MgHst, Parg, Tsch		
Tsch		
MgHst, Tsch, MgHbl		
Parg, Tsch		
MgHst, Parg		
MgHbl, Tsch		
MgHst, Tsch, MgHbl		
MgHbl		
MgHst, Tsch		
Tsch, Parg		

ıge 45.1 - 77.3 wt% SiO2 and 0.2 - 6.9 wt% MgO.

2012)'s and Erdmann et al. (2014)'s study.

Table 2 Results of multiple linear regressions used for estimating melt major element compositions on the

Eq.	Dependent variable	Parameters used	Range of variation	Constant		
					T ºC	Si
1	SiO_2 (wt %)	$lnSi_T$	39.6 - 79.2	-736.7170		
2	SiO_2 (wt %)	$lnSi_T$	39.6 - 79.2	-399.9891		
3	SiO_2 (wt %)	$lnSi_T$, Fe_T	39.6 - 79.2	-228.0000	**0.0107**	
4	SiO_2 (wt %)	$lnSi_T$, Fe_T	39.6 - 79.2	-222.6140		
5	$lnTiO_2$	Si_T	-2.8 - 1.8	23.4870	**-0.0011**	-2.5692
6	$lnTiO_2$	Si_T	-2.8 - 1.8	22.4650		-2.5975
7	ln FeO	Si_T	-0.34 - 2.75	24.4613		-2.7231
8	lnFeO	Si_T, Fe_T	-0.34 - 2.75	15.6864		-2.0966
9	lnMgO	Si_T	-2.19 - 2.47	12.6618		-2.6319
10	CaO (wt %)	Si_T	0.5 - 14.7	41.2784		-7.1955
11	lnCaO	Si_T	-0.7 - 2.7	6.4192		-1.1737
12	K_2O (wt %)	Si_T	<6.0	100.5909		-4.3246
13	K_2O (wt %)	Si_T, Fe_T	<6.0	-16.5300		1.6878
14	Al_2O_3 (wt %)	Si_T	11.4 - 21.5	4.5730		

Normal font indicates p-value < 0.01; bold font indicates the *p-value* of the parameter or the constant is 0.

basis of temperature and calcic-amphibole component. N = 130

Independent variable coefficients						
InSi	**Al (vi)**	**Mg**	**Fe3+**	**Fe2+**	**Fetot**	**Ti**
288.7330	56.5360	27.1690	62.6650	34.8140		83.9890
212.9463	11.7464		23.5653	6.8467		24.7743
165.0000		-7.2190				
167.5170		-7.1560				
	-1.3919		-2.1195	-1.0511		
	-1.1550		-2.2329	-1.0319		
	-1.0735		-1.0466	-0.2580		-1.9360
		0.3646				
	1.0500	1.2604				
		3.6412				
	1.3198	0.6773				
	-17.8256	-10.0901	-15.6830	-8.8004		-19.7448
					1.2354	5.0404
	6.9408	1.0059	4.5448			5.9679

01 ≤ *p-value* < 0.05

Ca	Na (A)	*Multiple R^2*	*SE (wt %)*	*se (wt%)*
44.2250	14.0490	0.849	3.29	3.78
24.4399		0.834	3.38	4.19
		0.791	3.70	4.37
		0.782	3.75	4.51
-2.0634	-1.5961	0.820	0.62	0.17
-1.9825	-1.5591	0.813	0.66	0.16
-2.5228		0.712	1.67	1.54
-1.3313		0.699	1.76	1.35
		0.798	0.96	0.64
	-5.0437	0.606	1.35	1.23
		0.711	1.31	1.43
-6.3727	-5.8069	0.630	0.59	0.78
2.9703		0.434	0.57	0.69
	7.1501	0.585	0.93	1.11

Table 3 Equilibrium test for pairs of amphibole rims and matrix glasses from pumice clasts in Ongatiti ignir

Pumice #		Am. wt %	Am.sd.	Gl. wt %	Gl.sd.	Pred. wt %	Pred.sd.	MR.se.	Diff.	Diff%	Diff.>MR.se?
GC1	SiO_2	44.62	0.33	77.75	0.16	77.37	0.82	3.59	-0.38	-0.5%	
(N.amph = 28)	TiO_2	1.77	0.04	0.13	0.02	0.11	0.01	0.66	-0.02	-14.5%	
(N.gl = 22)	Al_2O_3	7.68	0.16	12.34	0.11	13.61	0.11	1.13	1.27	10.3%	Y
	FeO	19.40	0.30	1.30	0.07	1.16	0.07	1.76	-0.14	-10.5%	
	MgO	10.17	0.19	0.11	0.01	0.13	0.01	0.95	0.02	21.9%	
	CaO	10.59	0.08	0.85	0.02	1.21	0.03	1.38	0.36	**41.8%**	
	K_2O	0.65	0.03	4.08	0.12	4.91	0.09	0.60	0.83	20.2%	Y
	Na_2O	1.98	0.05	3.41	0.17						
	MnO	0.48	0.03	0.04	0.02						
P2023	SiO_2	45.93	0.39	77.86	0.24	80.37	0.63	3.59	2.51	3.2%	
(N.amph = 15)	TiO_2	1.75	0.06	0.14	0.02	0.10	0.01	0.66	-0.04	-28.6%	
(N.gl = 28)	Al_2O_3	7.31	0.17	12.39	0.08	13.19	0.14	1.13	0.80	6.5%	
	FeO	19.33	0.64	1.20	0.19	0.95	0.04	1.76	-0.25	-20.8%	
	MgO	10.37	0.37	0.10	0.02	0.10	0.01	0.95	0.00	-1.4%	
	CaO	10.74	0.07	0.92	0.07	1.11	0.05	1.38	0.19	20.8%	
	K_2O	0.61	0.04	3.86	0.15	4.91	0.15	0.60	1.05	**27.3%**	Y
	Na_2O	1.81	0.06	3.50	0.11						
	MnO	0.41	0.02	0.03	0.02						
P2026	SiO_2	45.07	0.44	78.23	0.23	77.57	2.40	3.59	-0.66	-0.8%	
(N.amph = 5)	TiO_2	1.82	0.08	0.13	0.02	0.11	<0.01	0.66	-0.02	-16.2%	
(N.gl = 28)	Al_2O_3	7.48	0.18	12.30	0.07	13.27	0.08	1.13	0.97	7.8%	
	FeO	20.11	0.29	0.73	0.27	1.12	0.07	1.76	0.39	**53.6%**	
	MgO	10.45	0.22	0.05	0.03	0.13	0.01	0.95	0.08	**160.4%**	Y
	CaO	10.79	0.04	0.74	0.06	1.18	0.03	1.38	0.44	**59.8%**	Y
	K_2O	0.63	0.04	4.65	0.33	4.82	0.12	0.60	0.17	3.7%	
	Na_2O	1.92	0.06	3.15	0.20						
	MnO	0.44	0.02	0.01	0.01						
P2027	SiO_2	45.15	0.46	77.97	0.43	79.85	1.12	3.59	1.88	2.4%	
(N.amph = 33)	TiO_2	1.82	0.06	0.13	0.01	0.10	0.01	0.66	-0.03	23.0%	
(N.gl = 9)	Al_2O_3	7.23	0.22	12.50	0.14	13.10	0.19	1.13	0.60	4.8%	
	FeO	19.53	0.31	0.72	0.40	0.99	0.90	1.76	0.27	**37.6%**	
	MgO	10.24	0.25	0.04	0.03	0.11	0.01	0.95	0.07	**160.6%**	Y
	CaO	10.66	0.11	0.77	0.07	1.11	0.05	1.38	0.34	**43.2%**	Y
	K_2O	0.60	0.04	4.79	0.34	4.87	0.10	0.60	0.08	1.7%	
	Na_2O	1.78	0.09	3.06	0.19						
	MnO	0.37	0.02	0.01	0.01						
P2184	SiO_2	44.74	0.35	78.63	0.30	79.01	0.79	3.59	0.38	0.5%	
(N.amph = 30)	TiO_2	1.81	0.11	0.13	0.01	0.10	0.01	0.66	-0.03	24.0%	
(N.gl = 29)	Al_2O_3	7.60	0.26	12.21	0.08	13.34	0.28	1.13	1.13	9.3%	
	FeO	19.97	0.54	0.74	0.30	1.10	0.08	1.76	0.36	**48.4%**	
	MgO	9.95	0.31	0.06	0.03	0.12	0.02	0.95	0.06	**95.6%**	Y
	CaO	10.64	0.11	0.79	0.02	1.15	0.08	1.38	0.36	**44.9%**	Y
	K_2O	0.64	0.04	4.09	0.13	4.84	0.20	0.60	0.75	18.3%	
	Na_2O	1.83	0.06	3.32	0.13						
	MnO	0.38	0.02	0.02	0.01						

Compositions of amphibole rims and matrix glasses, as well as predicted melt in equilibrium with amphibole rims, are given as average values of multiple analyses from each pumice clast, with standard deviation; Diff. indicates the disparity between the predicted melt compositions and matrix glasses; Diff% = Diff./Gl. wt %; Diff% is highlighted in bold font when it is > 20.0%; Y indicates Diff. is larger than the se of the chemometric equation which is used for predicting melt compositions.

nbrite

Table 4 Results of Fe-Mg interdiffusion modelling carried out on amphiboles from pumice clasts of the Ongatiti ignimbrite

	Amphibole compositions	Originally predicted melt compositions	Melt compositions predicted using different Mg#					
			0.80	0.70	0.60	0.50	0.40	0.30
SiO_2	41.83	65.21	61.03	64.09	67.14	70.20	73.26	76.32
TiO_2	3.33	0.48	0.85	0.56	0.37	0.25	0.16	0.11
Al_2O_3	11.62	18.35	18.90	18.50	18.10	17.69	17.29	16.89
FeO_t	13.32	4.16	5.08	4.39	3.80	3.28	2.84	2.45
MgO	12.10	0.99	1.97	1.19	0.72	0.43	0.26	0.16
CaO	11.09	3.37	4.88	3.72	2.84	2.17	1.65	1.26
K_2O	0.43	2.53	1.82	2.34	2.85	3.37	3.89	4.40
SiO_2	44.65	77.42	67.77	71.16	74.55	77.93	81.32	84.71
TiO_2	1.82	0.11	0.41	0.26	0.16	0.10	0.07	0.04
Al_2O_3	7.66	13.49	14.75	14.30	13.86	13.41	12.97	12.52
FeO_t	19.70	1.14	1.80	1.53	1.30	1.11	0.94	0.80
MgO	10.00	0.13	0.62	0.35	0.20	0.12	0.07	0.04
CaO	10.64	1.20	2.83	2.09	1.55	1.15	0.85	0.63
K_2O	0.65	4.85	3.23	3.81	4.38	4.95	5.52	6.09

The first amphibole is a MgHst with 0.76 Mg#, 0.33 wt% MnO and 2.89 wt % Na_2O; the second amphibole is MgHbl with 0.53 Mg#, 0.42 wt% MnO and 1.98 wt % Na_2O.